

Electronic Supplementary Information for

Ligand Engineering of Tetra N-Heterocyclic Carbenes for Boosting Catalytic Aziridination

Brett A. Smith, Somon Hakimov, David M. Jenkins,* Konstantinos D. Vogiatzis*

*Department of Chemistry, University of Tennessee, Knoxville, Tennessee 37996-1600, United
States*

Email: djenki15@utk.edu, kvogiatz@utk.edu

Contents

| | |
|--|----|
| Section S1. Density Functional Benchmarking | 3 |
| Section S1.1. Computational Details, Convergence Criteria and Transition State Optimization | 6 |
| Section S2. Free Volume, Steric-Mapping, Key Bond Lengths and Tolman Electronic Parameters | 8 |
| Section S3. Frontier Molecular Orbital Analysis..... | 19 |
| Section S3.1. Orbital Energies and Orbital Energy Differences..... | 19 |
| Section S3.1. Molecular Orbital Visualization and Selected Spin Densities..... | 27 |
| Section S3.2 Spin Densities | 54 |

Section S1. Density Functional Benchmarking

The use of density functional theory in computational catalysis has become a common practice, but careful consideration and benchmarking is of great importance to any study utilizing DFT. Aziridination with iron tetra-NHC catalysts have been studied using DFT in previous studies¹, where various density functionals were benchmarked (see their ESI documents). Since the publication of this study four additional iron tetra-NHC crystal structures have been isolated,²⁻⁴ and we sought to re-evaluate the performance of various density functionals. Using the ORCA 5.0.2 software package⁵ we have evaluated the performance of the BLYP, BP86, OLYP, PBE, RPBE, TPSS and SCAN density functionals. All calculations utilized Grimme's D3 dispersion correction with Becke-Johnson damping^{6,7}, def2-SVP was used for all non-iron atoms, and def2-TZVP was used for iron.^{8,9} Key bond distances and bond angles were evaluated against the original crystal structure as a reference.

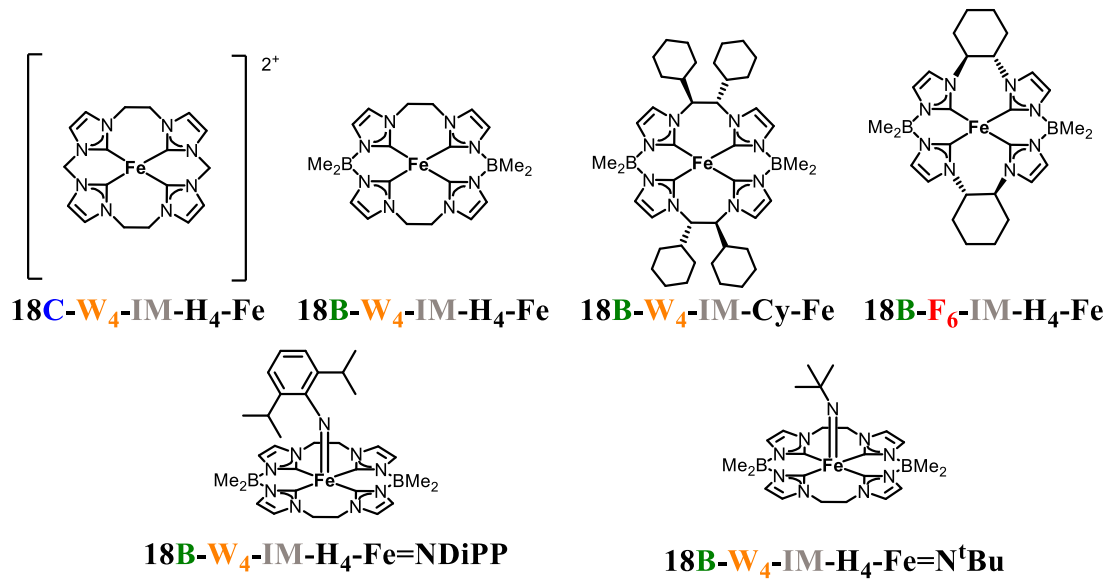


Figure S - 1. Selected geometries with experimentally refined crystal structures used for DFT benchmarking.

The key bond distances and angles for the crystal structures that are not intermediates (iron(IV)-imides) are shown in **Table S - 1**. The key bond distances and angles for the remaining to iron(IV)-imide crystal structures can be found in **Table S - 2**.

| Coordinate | 18C-W ₄ -IM-H ₄ - | 18B-W ₄ -IM-H ₄ - | 18B-W ₄ -IM-Cy ₄ - | 18B-F ₆ -IM-H ₄ - |
|-----------------------------------|---|---|--|---|
| | Fe | Fe | Fe | Fe |
| Fe-C ₁ | 2.052 | 1.941 | 2.046 | 1.951 |
| Fe-C ₂ | 1.986 | 1.941 | 1.984 | 2.006 |
| Fe-C ₃ | 2.029 | 1.943 | 1.992 | 1.938 |
| Fe-C ₄ | 1.977 | 1.934 | 2.031 | 2.005 |
| C ₁ -Fe-C ₃ | 3.286 | 3.461 | 3.379 | 3.477 |
| C ₂ -Fe-C ₄ | 3.287 | 3.439 | 3.384 | 3.351 |
| C ₁ -Fe-C ₂ | 1.931 | 179.197 | 171.291 | 120.193 |
| C ₃ -Fe-C ₄ | 1.917 | 178.265 | 167.254 | 157.593 |
| ^a E-Fe-E | 169.726 | 89.214 | 86.593 | 10.025 |

^aE denotes the group that links together the dicarbene subunits, either BMe₃ or CH₂

Table S - 1. Key bond distances and angles for the various crystal structures used in benchmarking, in Å and degrees.

| Coordinate | 18B-W ₄ -IM-H ₄ - | 18B-W ₄ -IM-H ₄ - |
|-----------------------------------|---|---|
| | Fe=N ^t Bu | Fe=NDiPP |
| Fe-C ₁ | 1.933 | 1.986 |
| Fe-C ₂ | 1.929 | 1.980 |
| Fe-C ₃ | 1.987 | 1.973 |
| Fe-C ₄ | 1.996 | 1.978 |
| Fe-N | 1.655 | 1.730 |
| Fe-N-R | 150.067 | 163.041 |
| C ₁ -Fe-C ₃ | 143.063 | 150.826 |
| C ₂ -Fe-C ₄ | 141.191 | 152.798 |
| C ₁ -Fe-C ₂ | 86.776 | 86.388 |
| C ₃ -Fe-C ₄ | 83.716 | 86.280 |
| ^a E-Fe-E | 109.083 | 129.001 |

^aE denotes the group that links together the dicarbene subunits, either BMe₃ or CH₂

Table S - 2. Key bond distances and angles for the various crystal imide structures used in benchmarking in Å and degrees

| Bond Angles (degrees) | | Bond Lengths (Å) | |
|-----------------------|----------|------------------|--------|
| Functional | MAE(deg) | Functional | MAE(Å) |
| BLYP | 3.00 | BLYP | 0.026 |
| BP86 | 2.03 | BP86 | 0.025 |
| OLYP | 3.22 | OLYP | 0.040 |
| PBE | 1.42 | PBE | 0.023 |
| Rpbe | 2.96 | Rpbe | 0.032 |
| TPSS | 2.96 | TPSS | 0.024 |
| SCANfunc | 3.37 | SCANfunc | 0.025 |

Table S - 3. Overall density functional mean absolute error in bond lengths (right) and bond angles (left).

The top performers are PBE-D3(BJ), TPSS-D3(BJ), and BP86-D3(BJ), with PBE-D3(BJ) providing the both the most accurate bond angles and bond lengths. This has led us to conclude TPSS and PBE provide the most accurate results, but due to its' computational efficiency, PBE was chosen as our density functional of choice.

Section S1.1. Computational Details, Convergence Criteria and Transition State Optimization

All geometry optimizations and frequency calculations were carried using the ORCA 5.0.2 software package^{1, 2}. All results shown herein were obtained with the PBE density functional³, along with Grimme's D3 dispersion correction with Becke-Johnson Damping (D3(BJ))^{4, 5} and the resolution of identity (RI)⁶. The def2-SVP basis set was used for all non-iron atoms, while iron employed the def2-TZVP basis set,^{7, 8} with matching auxiliary basis sets. All calculations were carried out with an intermediate spin-state ($S = 1$), as it is the predicted ground state from

DFT, multireference methods and experimental methods⁹⁻¹². Additionally the calculation of free volume was performed using SambVca 2.0¹³. All Natural Orbitals for Chemical Valence (NOCV) calculations were carried out in the Multiwfn software package¹⁴. In addition, the convergence criteria for the SCF and geometry optimization cycles are listed below:

| Criteria | Tolerance | Units |
|-------------------|-----------|-------------------|
| Energy Change | 5.00E-06 | E_h |
| Max. Gradient | 3.00E-04 | E_h/Bohr |
| RMS Gradient | 1.00E-04 | E_h/Bohr |
| Max. Displacement | 4.00E-03 | Bohr |
| RMS Displacement | 2.00E-03 | Bohr |

Table S 1. Convergence criteria

Identifying true minima in optimizations was done through analysing the vibrational frequencies for any imaginary frequencies. There were multiple approaches taken for identifying transition structures.

1. All transition structures began with a transition state relaxed surface scan of the internal coordinate of interest (ORCA keyword:ScanTS).

TS1: [Fe-N₁R=N₂=N₃] N₁-N₂ was scanned from 1.2 to 1.8 angstroms with 10 steps of 0.06 angstroms each.

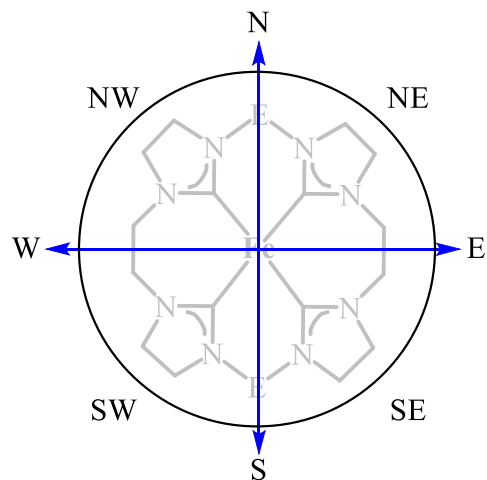
TS2: [Fe=N₁R--C_{Decene}] N₁--C_{decene} was scanned from 1.5 to 2.0 angstroms with 10 steps of 0.05 angstroms each.

TS3: [Fe-N₁-C_{Tolyl}-C_{Decene}] the angle N₁-C_{Tolyl}-C_{Decene} was scanned from 95 degrees to 55 degrees of steps of 2 degrees each

2. Each transition structure was further relaxed with a transition state optimization (ORCA
Keyword: OptTS) using the same energy and geometry tolerances.
3. Manual inspection to ensure a single imaginary frequency and visual inspection of the
vibrational mode to ensure expected stretches/bends.

Section S2. Free Volume, Steric-Mapping, Key Bond Lengths and Tolman Electronic Parameters

Free/Buried volume calculations have been used as a steric descriptor extensively for transition metal complexes with carbene ligands.



Scheme S - 1. Representation of the decomposition of regions for quadrant analysis, as an example 18E-W₄-IN-H₄-Fe has been shown.

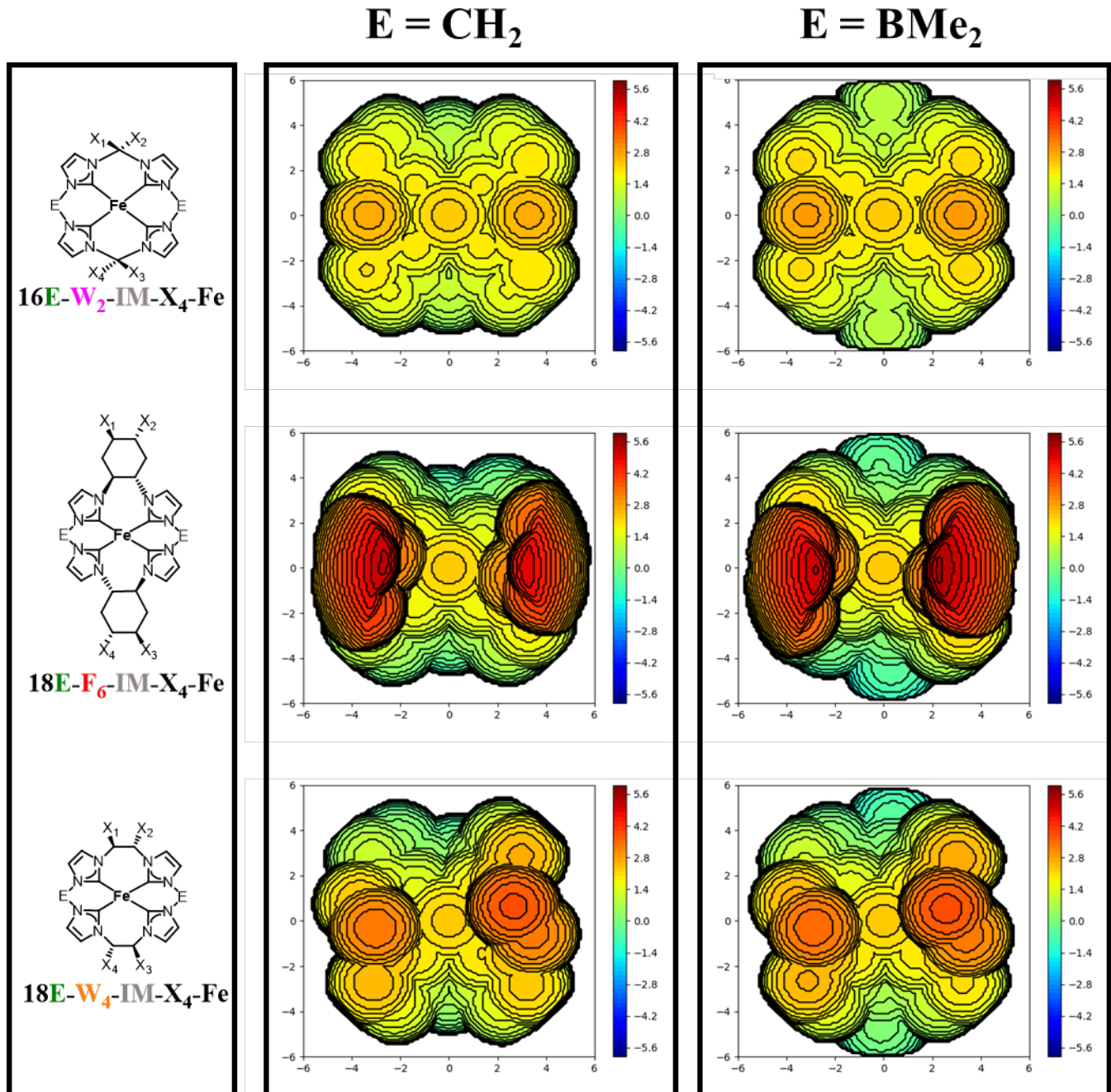


Figure S - 2. Steric mapping of complexes containing imidazole (IM) carbene subunits. Left panel showing the chemical structures, where the “E” can be either CH_2 (center panel) or BMe_2 (right panel). Steric maps shown for 16E-W₂-IM-H₄-Fe (top), 18E-F₆-IM-H₄-Fe (middle) and 18E-W₄-IM-H₄-Fe (bottom).

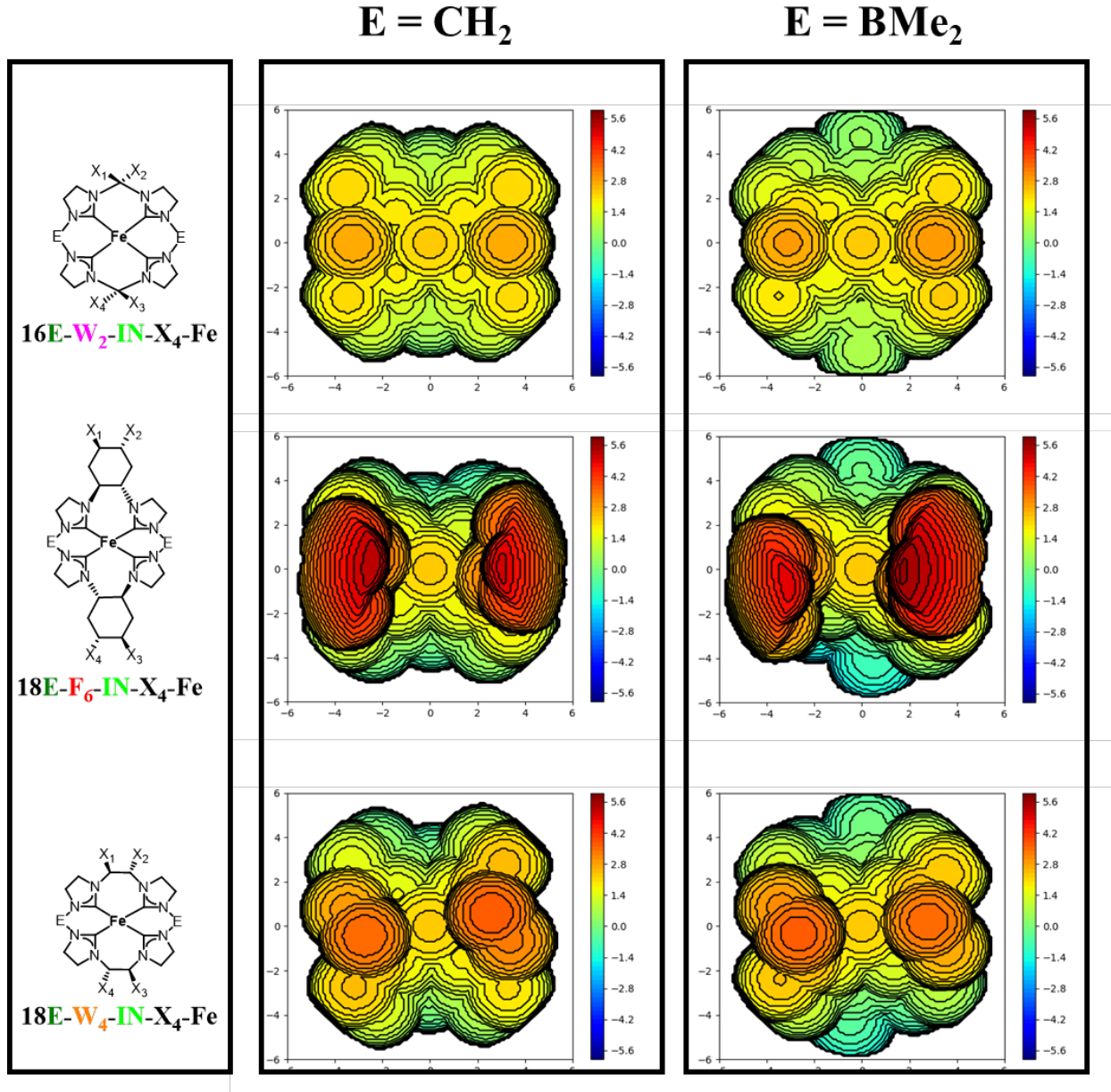


Figure S - 3. Steric mapping of complexes containing imidazole (IM) carbene subunits. Left panel showing the chemical structures, where the “E” can be either \mathbf{CH}_2 (center panel) or \mathbf{BMe}_2 (right panel). Steric maps shown for 16E-W₂-IM-H₄-Fe (top), 18E-F₆-IM-H₄-Fe (middle) and 18E-W₄-IM-H₄-Fe (bottom).

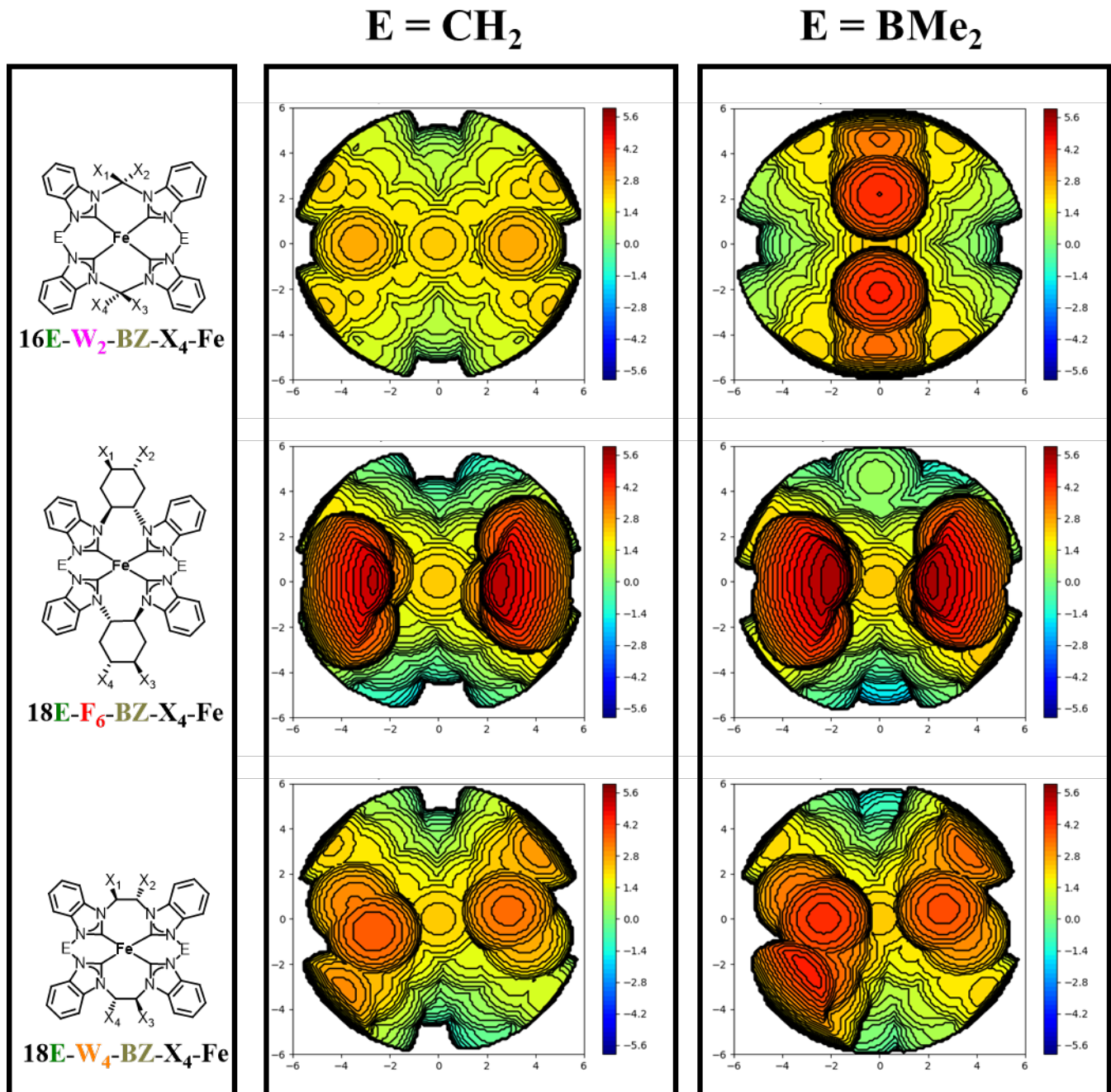


Figure S - 4. Steric mapping of complexes containing imidazole (IM) carbene subunits. Left panel showing the chemical structures, where the “E” can be either CH₂ (center panel) or BMe₂

(right panel). Steric maps shown for 16E-W₂-IM-H₄-Fe (top), 18E-F₆-IM-H₄-Fe (middle) and 18E-W₄-IM-H₄-Fe (bottom).

| Complex | V _{Free} (Å ³) | V _{Buried} (Å ³) | V _{Total} (Å ³) | %V _{Free} | %V _{Buried} |
|---|-------------------------------------|---------------------------------------|--------------------------------------|--------------------|----------------------|
| 16C-W ₂ -IM-H ₄ -Fe | 562.9 | 341.1 | 904 | 62.3 | 37.7 |
| 18C-W ₄ -IM-H ₄ -Fe | 529.8 | 374.2 | 904 | 58.6 | 41.4 |
| 18C-F ₆ -IM-H ₄ -Fe | 470.4 | 433.6 | 904 | 52 | 48 |
| 16B-W ₂ -IM-H ₄ -Fe | 498.2 | 405.8 | 904 | 55.1 | 44.9 |
| 18B-W ₄ -IM-H ₄ -Fe | 465.7 | 438.3 | 904 | 51.5 | 48.5 |
| 18B-F ₆ -IM-H ₄ -Fe | 400.3 | 503.7 | 904 | 44.3 | 55.7 |
| 16C-W ₂ -IN-H ₄ -Fe | 554.9 | 349.1 | 904 | 61.4 | 38.6 |
| 18C-W ₄ -IN-H ₄ -Fe | 522.2 | 381.8 | 904 | 57.8 | 42.2 |
| 18C-F ₆ -IN-H ₄ -Fe | 457.4 | 446.7 | 904 | 50.6 | 49.4 |
| 16B-W ₂ -IN-H ₄ -Fe | 488.6 | 415.4 | 904 | 54.0 | 46.0 |
| 18B-W ₄ -IN-H ₄ -Fe | 455.7 | 448.3 | 904 | 50.4 | 49.6 |
| 18B-F ₆ -IN-H ₄ -Fe | 380.3 | 523.7 | 904 | 42.1 | 57.9 |
| 16C-W ₂ -BZ-H ₄ -Fe | 526.1 | 377.9 | 904 | 58.2 | 41.8 |
| 18C-W ₄ -BZ-H ₄ -Fe | 495.5 | 408.5 | 904 | 54.8 | 45.2 |
| 18C-F ₆ -BZ-H ₄ -Fe | 424.6 | 479.4 | 904 | 47.0 | 53.0 |
| 16B-W ₂ -BZ-H ₄ -Fe | 461.9 | 442.2 | 904 | 51.1 | 48.9 |
| 18B-W ₄ -BZ-H ₄ -Fe | 431.1 | 473 | 904 | 47.7 | 52.3 |
| 18B-F ₆ -IN-H ₄ -Fe | 352.5 | 551.5 | 904 | 39.0 | 61.0 |

Table S - 4. Tabulated values from steric mapping and analysis. V_{Free}, V_{Buried} and V_{Total} are all shown in units of Å³ and represent that calculated volumes. The percentage of free volume and buried volume are percentages in comparison to the total volumes. The total volume for each molecule is identical at 904 Å³, which is a result of the chosen sphere radius.

| 16C-W₂-IM-H₄-Fe | | | | |
|--|-------------------------------------|---------------------------------------|--------------------------------------|--------------------|
| Quadrant | V _{Free} (Å ³) | V _{Buried} (Å ³) | V _{Total} (Å ³) | %V _{Free} |
| SW | 140.8 | 85.2 | 226 | 62.3 |
| NW | 140.6 | 85.4 | 226 | 62.2 |
| NE | 140.6 | 85.4 | 226 | 62.2 |
| SE | 140.9 | 85.1 | 226 | 62.3 |
| 18C-W₄-IM-H₄-Fe | | | | |
| Quadrant | V _{Free} (Å ³) | V _{Buried} (Å ³) | V _{Total} (Å ³) | %V _{Free} |
| SW | 135.4 | 90.6 | 226 | 59.9 |
| NW | 132.7 | 93.3 | 226 | 58.7 |
| NE | 128.5 | 97.5 | 226 | 56.9 |

| | | | | |
|--|-------------------------------------|---------------------------------------|--------------------------------------|--------------------|
| SE | 133.1 | 92.9 | 226 | 58.9 |
| 18C-F₆-IM-H₄-Fe | | | | |
| Quadrant | V _{Free} (Å ³) | V _{Buried} (Å ³) | V _{Total} (Å ³) | %V _{Free} |
| SW | 115.8 | 110.2 | 226 | 51.2 |
| NW | 117.3 | 108.7 | 226 | 51.9 |
| NE | 114.5 | 111.5 | 226 | 50.7 |
| SE | 122.7 | 103.3 | 226 | 54.3 |
| 16B-W₂-IM-H₄-Fe | | | | |
| Quadrant | V _{Free} (Å ³) | V _{Buried} (Å ³) | V _{Total} (Å ³) | %V _{Free} |
| SW | 124.7 | 101.3 | 226 | 55.2 |
| NW | 124.7 | 101.3 | 226 | 55.2 |
| NE | 124.5 | 101.5 | 226 | 55.1 |
| SE | 124.3 | 101.7 | 226 | 55 |
| 18B-W₄-IM-H₄-Fe | | | | |
| Quadrant | V _{Free} (Å ³) | V _{Buried} (Å ³) | V _{Total} (Å ³) | %V _{Free} |
| SW | 116.6 | 109.4 | 226 | 51.6 |
| NW | 122.8 | 103.2 | 226 | 54.3 |
| NE | 107.6 | 118.4 | 226 | 47.6 |
| SE | 118.7 | 107.3 | 226 | 52.5 |
| 18B-F₆-IM-H₄-Fe | | | | |
| Quadrant | V _{Free} (Å ³) | V _{Buried} (Å ³) | V _{Total} (Å ³) | %V _{Free} |
| SW | 101.8 | 124.2 | 226 | 45 |
| NW | 103 | 123 | 226 | 45.6 |
| NE | 100 | 126 | 226 | 44.3 |
| SE | 95.6 | 130.4 | 226 | 42.3 |

Table S - 5. Steric analysis of IM based complexes, where quadrants decompose the steric map into four regions, Southwest (SW), Northwest(NW), Northeast (NE) and Southeast (SE).

| | | | | |
|--|-------------------------------------|---------------------------------------|--------------------------------------|--------------------|
| 16C-W₂-IN-H₄-Fe | | | | |
| Quadrant | V _{Free} (Å ³) | V _{Buried} (Å ³) | V _{Total} (Å ³) | %V _{Free} |
| SW | 138.6 | 87.4 | 226 | 61.3 |
| NW | 138.8 | 87.2 | 226 | 61.4 |
| NE | 138.9 | 87.1 | 226 | 61.4 |
| SE | 138.6 | 87.4 | 226 | 61.3 |
| 18C-W₄-IN-H₄-Fe | | | | |
| Quadrant | V _{Free} (Å ³) | V _{Buried} (Å ³) | V _{Total} (Å ³) | %V _{Free} |
| SW | 132 | 94 | 226 | 58.4 |
| NW | 130.7 | 95.3 | 226 | 57.8 |
| NE | 128.8 | 97.2 | 226 | 57 |
| SE | 130.7 | 95.3 | 226 | 57.8 |
| 18C-F₆-IN-H₄-Fe | | | | |
| Quadrant | V _{Free} (Å ³) | V _{Buried} (Å ³) | V _{Total} (Å ³) | %V _{Free} |
| SW | 112.6 | 113.4 | 226 | 49.8 |

| NW | 113.6 | 112.4 | 226 | 50.2 |
|--|-------------------------------------|---------------------------------------|--------------------------------------|--------------------|
| NE | 110.6 | 115.5 | 226 | 48.9 |
| SE | 120.6 | 105.4 | 226 | 53.4 |
| 16B-W₂-IN-H₄-Fe | | | | |
| Quadrant | V _{Free} (Å ³) | V _{Buried} (Å ³) | V _{Total} (Å ³) | %V _{Free} |
| SW | 123.4 | 102.6 | 226 | 54.6 |
| NW | 122.7 | 103.3 | 226 | 54.3 |
| NE | 121.2 | 104.8 | 226 | 53.6 |
| SE | 121.3 | 104.7 | 226 | 53.7 |
| 18B-W₄-IN-H₄-Fe | | | | |
| Quadrant | V _{Free} (Å ³) | V _{Buried} (Å ³) | V _{Total} (Å ³) | %V _{Free} |
| SW | 106.3 | 119.7 | 226 | 47 |
| NW | 118 | 108 | 226 | 52.2 |
| NE | 110.5 | 115.5 | 226 | 48.9 |
| SE | 120.9 | 105.1 | 226 | 53.5 |
| 18B-F₆-IN-H₄-Fe | | | | |
| Quadrant | V _{Free} (Å ³) | V _{Buried} (Å ³) | V _{Total} (Å ³) | %V _{Free} |
| SW | 97.7 | 128.3 | 226 | 43.3 |
| NW | 105.3 | 120.7 | 226 | 46.6 |
| NE | 92.4 | 133.6 | 226 | 40.9 |
| SE | 84.8 | 141.2 | 226 | 37.5 |

Table S - 6. Steric analysis of IN complexes, where quadrants decompose the steric map into four regions, Southwest (SW), Northwest(NW), Northeast (NE) and Southeast (SE).

| 16C-W₂-BZ-H₄-Fe | | | | |
|--|-------------------------------------|---------------------------------------|--------------------------------------|--------------------|
| Quadrant | V _{Free} (Å ³) | V _{Buried} (Å ³) | V _{Total} (Å ³) | %V _{Free} |
| SW | 131.5 | 94.5 | 226 | 58.2 |
| NW | 131.5 | 94.5 | 226 | 58.2 |
| NE | 131.5 | 94.5 | 226 | 58.2 |
| SE | 131.5 | 94.5 | 226 | 58.2 |
| 18C-W₄-BZ-H₄-Fe | | | | |
| Quadrant | V _{Free} (Å ³) | V _{Buried} (Å ³) | V _{Total} (Å ³) | %V _{Free} |
| SW | 121.2 | 104.8 | 226 | 53.6 |
| NW | 124.5 | 101.5 | 226 | 55.1 |
| NE | 125.3 | 100.7 | 226 | 55.5 |
| SE | 124.4 | 101.6 | 226 | 55.1 |
| 18C-F₆-BZ-H₄-Fe | | | | |
| Quadrant | V _{Free} (Å ³) | V _{Buried} (Å ³) | V _{Total} (Å ³) | %V _{Free} |
| SW | 89.9 | 136.1 | 226 | 39.8 |
| NW | 85 | 141 | 226 | 37.6 |
| NE | 84.8 | 141.2 | 226 | 37.5 |
| SE | 92.8 | 133.2 | 226 | 41 |
| 16B-W₂-BZ-H₄-Fe | | | | |

| Quadrant | V _{Free} (Å ³) | V _{Buried} (Å ³) | V _{Total} (Å ³) | %V _{Free} |
|--|-------------------------------------|---------------------------------------|--------------------------------------|--------------------|
| SW | 115.3 | 110.7 | 226 | 51 |
| NW | 115.7 | 110.3 | 226 | 51.2 |
| NE | 115.5 | 110.5 | 226 | 51.1 |
| SE | 115.3 | 110.7 | 226 | 51 |
| 18B-W₄-BZ-H₄-Fe | | | | |
| Quadrant | V _{Free} (Å ³) | V _{Buried} (Å ³) | V _{Total} (Å ³) | %V _{Free} |
| SW | 100.6 | 125.5 | 226 | 44.5 |
| NW | 109.5 | 116.5 | 226 | 48.5 |
| NE | 102.1 | 123.9 | 226 | 45.2 |
| SE | 118.8 | 107.2 | 226 | 52.6 |
| 18B-F₆-IN-H₄-Fe | | | | |
| Quadrant | V _{Free} (Å ³) | V _{Buried} (Å ³) | V _{Total} (Å ³) | %V _{Free} |
| SW | 89.9 | 136.1 | 226 | 39.8 |
| NW | 85 | 141 | 226 | 37.6 |
| NE | 84.8 | 141.2 | 226 | 37.5 |
| SE | 92.8 | 133.2 | 226 | 41 |

Table S - 7. Steric analysis of BZ complexes , where quadrants decompose the steric map into four regions, Southwest (SW), Northwest(NW), Northeast (NE) and Southeast (SE).

| Complex | μ(Fe-Carbene) (Å) | Fe=N (Å) | Fe=N-Tolyl (degrees) |
|---|-------------------|----------|----------------------|
| 16B-W ₂ -IM-H ₄ -Fe | 1.945 | 1.707 | 145.56 |
| 16C-W ₂ -IM-H ₄ -Fe | 1.929 | 1.718 | 156.46 |
| 18B-F ₆ -IM-H ₄ -Fe | 1.975 | 1.713 | 142.58 |
| 18C-F ₆ -IM-H ₄ -Fe | 1.958 | 1.711 | 149.34 |
| 18B-W ₄ -IM-H ₄ -Fe | 1.977 | 1.713 | 143.33 |
| 18C-W ₄ -IM-H ₄ -Fe | 1.969 | 1.716 | 149.58 |
| 16B-W ₂ -IN-H ₄ -Fe | 1.958 | 1.701 | 148.3 |
| 16C-W ₂ -IN-H ₄ -Fe | 1.949 | 1.715 | 153.82 |
| 18B-F ₆ -IN-H ₄ -Fe | 1.970 | 1.713 | 144.87 |
| 18C-F ₆ -IN-H ₄ -Fe | 1.964 | 1.707 | 149.88 |
| 18B-W ₄ -IN-H ₄ -Fe | 1.967 | 1.712 | 145.11 |
| 18C-W ₄ -IN-H ₄ -Fe | 1.971 | 1.712 | 149.26 |

| | | | |
|---|-------|-------|--------|
| 16B-W ₂ -BZ-H ₄ -Fe | 1.943 | 1.710 | 144.85 |
| 16C-W ₂ -BZ-H ₄ -Fe | 1.931 | 1.716 | 154.61 |
| 18B-F ₆ -BZ-H ₄ -Fe | 1.982 | 1.716 | 142.03 |
| 18C-F ₆ -BZ-H ₄ -Fe | 1.961 | 1.711 | 150.64 |
| 18B-W ₄ -BZ-H ₄ -Fe | 1.977 | 1.716 | 144.13 |
| 18C-W ₄ -BZ-H ₄ -Fe | 1.965 | 1.716 | 148.82 |

Table S - 8. Key bond lengths and distances for the iron(IV) imide intermediate.

| Complex | Fe=N (Å) | Fe=N-Tolyl (Å) | N-Radical (Å) | V _{imaginary} (cm ⁻¹) |
|---|----------|----------------|---------------|--|
| 16B-W ₂ -IM-H ₄ -Fe | 1.823 | 126.55 | 1.870 | (i)639.8 |
| 16C-W ₂ -IM-H ₄ -Fe | 1.794 | 127.02 | 1.917 | (i)457.3 |
| 18B-F ₆ -IM-H ₄ -Fe | 1.787 | 130.70 | 1.858 | (i)553.4 |
| 18C-F ₆ -IM-H ₄ -Fe | 1.821 | 131.01 | 1.947 | (i)522.0 |
| 18B-W ₄ -IM-H ₄ -Fe | 1.801 | 129.30 | 1.865 | (i)572.6 |
| 18C-W ₄ -IM-H ₄ -Fe | 1.817 | 132.82 | 1.920 | (i)427.1 |
| 16B-W ₂ -IN-H ₄ -Fe | 1.811 | 127.56 | 1.882 | (i)492.9 |
| 16C-W ₂ -IN-H ₄ -Fe | 1.794 | 129.12 | 1.924 | (i)450.6 |
| 18B-F ₆ -IN-H ₄ -Fe | 1.781 | 130.27 | 1.862 | (i)555.7 |
| 18C-F ₆ -IN-H ₄ -Fe | 1.821 | 130.04 | 1.941 | (i)465.2 |
| 18B-W ₄ -IN-H ₄ -Fe | 1.823 | 127.42 | 1.862 | (i)440.3 |
| 18C-W ₄ -IN-H ₄ -Fe | 1.806 | 129.90 | 1.929 | (i)431.9 |
| 16B-W ₂ -BZ-H ₄ -Fe | 1.792 | 127.62 | 1.862 | (i)443.9 |
| 16C-W ₂ -BZ-H ₄ -Fe | 1.793 | 128.49 | 1.938 | (i)437.2 |
| 18B-F ₆ -BZ-H ₄ -Fe | 1.788 | 130.97 | 1.893 | (i)548.8 |

| | | | | |
|---|-------|--------|-------|----------|
| 18C-F ₆ -BZ-H ₄ -Fe | 1.823 | 130.27 | 1.957 | (i)472.4 |
| 18B-W ₄ -BZ-H ₄ -Fe | 1.846 | 126.47 | 1.891 | (i)476.1 |
| 18C-W ₄ -BZ-H ₄ -Fe | 1.808 | 129.8 | 1.930 | (i)435.9 |

Table S - 9. Tabulated key bond lengths (\AA), bond angles (degrees) for the iron(IV)-imide species and the activated complex (TS_2). Additionally, the imaginary frequency corresponding to the N-C_{radical} bond formation for TS_2 is included, values displayed in cm^{-1} .

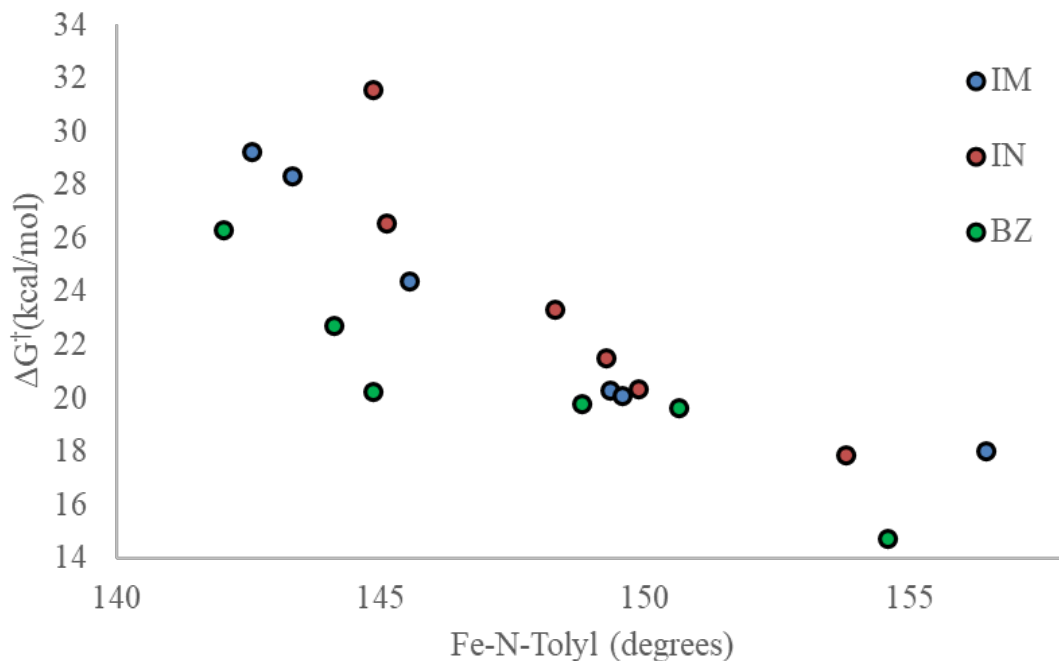


Figure S - 5. Scatter plot of the Fe=N-Tolyl bond angle vs ΔG^\dagger , with imidazole subunits in blue, imidazoline subunits in red and benzimidazole subunits in green.

| Complex | $\nu_{\text{CO}} (\text{cm}^{-1})$ |
|---|------------------------------------|
| 18B-F ₆ -BZ-H ₄ -Fe | 1887.27 |
| 18B-W ₄ -BZ-H ₄ -Fe | 1924.10 |
| 16B-W ₂ -BZ-H ₄ -Fe | 1964.60 |
| 18C-F ₆ -BZ-H ₄ -Fe | 1973.42 |
| 18C-W ₄ -BZ-H ₄ -Fe | 1993.36 |
| 16C-W ₂ -BZ-H ₄ -Fe | 2031.24 |
| 18B-F ₆ -IM-H ₄ -Fe | 1890.20 |
| 18B-W ₄ -IM-H ₄ -Fe | 1914.06 |
| 16B-W ₂ -IM-H ₄ -Fe | 1955.48 |
| 18C-F ₆ -IM-H ₄ -Fe | 1983.99 |
| 18C-W ₄ -IM-H ₄ -Fe | 1999.98 |
| 16C-W ₂ -IM-H ₄ -Fe | 2036.72 |
| 18B-F ₆ -IN-H ₄ -Fe | 1909.26 |
| 18B-W ₄ -IN-H ₄ -Fe | 1926.57 |
| 16B-W ₂ -IN-H ₄ -Fe | 1959.93 |
| 18C-F ₆ -IN-H ₄ -Fe | 1988.34 |
| 18C-W ₄ -IN-H ₄ -Fe | 1999.97 |
| 16C-W ₂ -IN-H ₄ -Fe | 2043.17 |

Table S - 10. Calculated vibrational frequencies for the A₁ carbonyl stretching vibration in cm⁻¹.

Section S3. Frontier Molecular Orbital Analysis

Section S3.1. Orbital Energies and Orbital Energy Differences.

| Complex | 16C-W ₂ -IM-H ₄ -Fe | 18C-W ₄ -IM-H ₄ -Fe | 18C-F ₆ -IM-H ₄ -Fe |
|--------------------|---|---|---|
| (α)HOMO-5 | -11.54 | -11.46 | -11.25 |
| (α)HOMO-4 | -11.50 | -11.35 | -11.17 |
| (α)HOMO-3 | -10.97 | -10.96 | -10.76 |
| (α)HOMO-2 | -10.85 | -10.83 | -10.64 |
| (α)HOMO-1 | -10.08 | -10.34 | -10.16 |
| (α)HOMO | -9.20 | -9.20 | -8.97 |
| (α)LUMO | -8.90 | -8.86 | -8.64 |
| (α)LUMO+1 | -6.79 | -6.77 | -6.63 |
| (β)HOMO-3 | -11.51 | -11.28 | -11.09 |
| (β)HOMO-2 | -11.04 | -11.20 | -11.06 |
| (β)HOMO-1 | -10.57 | -10.48 | -10.27 |
| (β)HOMO | -10.28 | -10.20 | -10.02 |
| (β)LUMO | -8.93 | -8.94 | -8.78 |
| (β)LUMO+1 | -8.56 | -8.45 | -8.23 |
| (β)LUMO+2 | -8.05 | -8.18 | -8.01 |
| Complex | 16B-W ₂ -IM-H ₄ -Fe | 18B-W ₄ -IM-H ₄ -Fe | 18B-F ₆ -IM-H ₄ -Fe |
| (α)HOMO-5 | -5.56 | -5.37 | -5.30 |
| (α)HOMO-4 | -5.34 | -5.29 | -5.24 |
| (α)HOMO-3 | -5.20 | -5.21 | -5.16 |
| (α)HOMO-2 | -4.81 | -4.68 | -4.61 |
| (α)HOMO-1 | -4.24 | -4.35 | -4.28 |
| (α)HOMO | -3.30 | -3.43 | -3.42 |
| (α)LUMO | -2.77 | -2.64 | -2.60 |
| (α)LUMO+1 | -0.74 | -0.86 | -0.94 |
| (β)HOMO-3 | -5.54 | -5.34 | -5.25 |
| (β)HOMO-2 | -5.21 | -5.12 | -5.08 |
| (β)HOMO-1 | -4.64 | -4.70 | -4.69 |
| (β)HOMO | -4.15 | -4.01 | -3.96 |
| (β)LUMO | -2.86 | -2.83 | -2.78 |
| (β)LUMO+1 | -2.40 | -2.51 | -2.51 |
| (β)LUMO+2 | -2.32 | -2.15 | -2.11 |

Table S - 11. Orbital energies from DFT optimization of the imidazole(IM) based Iron(IV)-imide species. All values listed in eV.

| Complex | 16C-W ₂ -IN-H ₄ -Fe | 18C-W ₄ -IN-H ₄ -Fe | 18C-F6-IN-H ₄ -Fe |
|--------------------|---|---|------------------------------|
| (α)HOMO-5 | -11.26 | -11.13 | -10.93 |
| (α)HOMO-4 | -11.12 | -11.08 | -10.84 |
| (α)HOMO-3 | -11.00 | -10.95 | -10.75 |
| (α)HOMO-2 | -10.94 | -10.91 | -10.70 |
| (α)HOMO-1 | -10.26 | -10.48 | -10.29 |
| (α)HOMO | -9.23 | -9.12 | -8.92 |
| (α)LUMO | -8.95 | -8.78 | -8.59 |
| (α)LUMO+1 | -6.69 | -6.77 | -6.68 |
| (β)HOMO-3 | -11.23 | -11.06 | -10.84 |
| (β)HOMO-2 | -11.09 | -10.95 | -10.75 |
| (β)HOMO-1 | -10.65 | -10.46 | -10.26 |
| (β)HOMO | -10.26 | -10.43 | -10.26 |
| (β)LUMO | -8.93 | -8.95 | -8.77 |
| (β)LUMO+1 | -8.59 | -8.37 | -8.17 |
| (β)LUMO+2 | -8.09 | -8.13 | -7.99 |
| Complex | 16B-W ₂ -IN-H ₄ -Fe | 18B-W ₄ -IN-H ₄ -Fe | 18B-F6-IN-H ₄ -Fe |
| (α)HOMO-5 | -5.10 | -4.97 | -4.91 |
| (α)HOMO-4 | -5.06 | -4.90 | -4.84 |
| (α)HOMO-3 | -4.85 | -4.77 | -4.72 |
| (α)HOMO-2 | -4.67 | -4.54 | -4.48 |
| (α)HOMO-1 | -4.26 | -4.28 | -4.21 |
| (α)HOMO | -3.30 | -3.32 | -3.34 |
| (α)LUMO | -2.70 | -2.45 | -2.47 |
| (α)LUMO+1 | -0.78 | -0.83 | -0.89 |
| (β)HOMO-3 | -4.92 | -4.72 | -4.66 |
| (β)HOMO-2 | -4.78 | -4.66 | -4.61 |
| (β)HOMO-1 | -4.65 | -4.51 | -4.46 |
| (β)HOMO | -4.18 | -4.16 | -4.13 |
| (β)LUMO | -2.88 | -2.80 | -2.74 |
| (β)LUMO+1 | -2.43 | -2.45 | -2.47 |
| (β)LUMO+2 | -2.24 | -1.97 | -1.97 |

Table S - 12. Orbital energies from DFT optimization of the imidazoline(IN) based Iron(IV)-imide species. All values listed in eV.

| Complex | 16C-W ₂ -BZ-H ₄ -Fe | 18C-W ₄ -BZ-H ₄ -Fe | 18C-F6-BZ-H ₄ -Fe |
|--------------------|---|---|------------------------------|
| (α)HOMO-5 | -10.93 | -10.84 | -10.70 |
| (α)HOMO-4 | -10.87 | -10.81 | -10.67 |
| (α)HOMO-3 | -10.68 | -10.69 | -10.53 |
| (α)HOMO-2 | -10.57 | -10.54 | -10.42 |
| (α)HOMO-1 | -9.85 | -10.12 | -9.97 |
| (α)HOMO | -8.97 | -8.96 | -8.83 |

| (α)LUMO | -8.68 | -8.63 | -8.50 |
|--------------------|---|---|------------------------------|
| (α)LUMO+1 | -6.88 | -6.86 | -6.80 |
| (β)HOMO-3 | -10.90 | -10.80 | -10.66 |
| (β)HOMO-2 | -10.66 | -10.73 | -10.60 |
| (β)HOMO-1 | -10.34 | -10.25 | -10.12 |
| (β)HOMO | -10.02 | -9.98 | -9.85 |
| (β)LUMO | -8.74 | -8.76 | -8.64 |
| (β)LUMO+1 | -8.35 | -8.22 | -8.10 |
| (β)LUMO+2 | -7.87 | -7.98 | -7.88 |
| Complex | 16B-W ₂ -BZ-H ₄ -Fe | 18B-W ₄ -BZ-H ₄ -Fe | 18B-F6-BZ-H ₄ -Fe |
| (α)HOMO-5 | -5.64 | -5.51 | -5.49 |
| (α)HOMO-4 | -5.52 | -5.50 | -5.45 |
| (α)HOMO-3 | -5.46 | -5.33 | -5.19 |
| (α)HOMO-2 | -5.15 | -5.07 | -4.95 |
| (α)HOMO-1 | -4.59 | -4.73 | -4.62 |
| (α)HOMO | -3.65 | -3.80 | -3.80 |
| (α)LUMO | -3.16 | -3.02 | -2.92 |
| (α)LUMO+1 | -1.62 | -1.52 | -1.55 |
| (β)HOMO-3 | -5.59 | -5.47 | -5.42 |
| (β)HOMO-2 | -5.42 | -5.31 | -5.18 |
| (β)HOMO-1 | -5.00 | -5.04 | -5.04 |
| (β)HOMO | -4.53 | -4.45 | -4.37 |
| (β)LUMO | -3.23 | -3.21 | -3.13 |
| (β)LUMO+1 | -2.79 | -2.89 | -2.92 |
| (β)LUMO+2 | -2.73 | -2.55 | -2.45 |

Table S - 13. Orbital energies from DFT optimization of the benzimidazole (BZ) based Iron(IV)-imide species. All values listed in eV.

| Complex | $\Delta E_{H(\alpha)-L(\alpha)}$ | $\Delta E_{H(\beta)-L(\beta)}$ | $\Delta E_{H(\alpha)-L(\beta)}$ | $\Delta E_{L(\alpha)-L(\beta)}$ | $\Delta E_{\sigma^*(\alpha)-\pi^*(\beta)}$ | $\Delta G_{\text{Act}}^\ddagger$ |
|---|----------------------------------|--------------------------------|---------------------------------|---------------------------------|--|----------------------------------|
| 16B-W ₂ -IM-H ₄ -Fe | -0.525 | -1.289 | -0.436 | 0.089 | -0.451 | 24.40 |
| 16C-W ₂ -IM-H ₄ -Fe | -0.294 | -1.344 | -0.265 | 0.029 | -0.343 | 18.21 |
| 18B-F ₆ -IM-H ₄ -Fe | -0.817 | -1.180 | -0.642 | 0.175 | -0.498 | 29.16 |
| 18C-F ₆ -IM-H ₄ -Fe | -0.325 | -1.243 | -0.190 | 0.134 | -0.411 | 20.30 |
| 18B-W ₄ -IM-H ₄ -Fe | -0.790 | -1.186 | -0.602 | 0.188 | -0.494 | 28.35 |
| 18C-W ₄ -IM-H ₄ -Fe | -0.342 | -1.266 | -0.265 | 0.077 | -0.408 | 20.07 |
| 16B-W ₂ -IN-H ₄ -Fe | -0.597 | -1.303 | -0.422 | 0.175 | -0.466 | 23.35 |
| 16C-W ₂ -IN-H ₄ -Fe | -0.279 | -1.326 | -0.297 | -0.018 | -0.361 | 17.78 |
| 18B-F ₆ -IN-H ₄ -Fe | -0.868 | -1.384 | -0.598 | 0.270 | -0.502 | 31.58 |
| 18C-F ₆ -IN-H ₄ -Fe | -0.327 | -1.483 | -0.148 | 0.179 | -0.420 | 20.36 |
| 18B-W ₄ -IN-H ₄ -Fe | -0.871 | -1.362 | -0.523 | 0.348 | -0.481 | 26.60 |
| 18C-W ₄ -IN-H ₄ -Fe | -0.342 | -1.485 | -0.175 | 0.167 | -0.411 | 21.51 |
| 16B-W ₂ -BZ-H ₄ -Fe | -0.491 | -1.295 | -0.424 | 0.067 | -0.438 | 20.23 |
| 16C-W ₂ -BZ-H ₄ -Fe | -0.289 | -1.276 | -0.228 | 0.062 | -0.337 | 14.75 |
| 18B-F ₆ -BZ-H ₄ -Fe | -0.875 | -1.240 | -0.668 | 0.207 | -0.474 | 26.28 |
| 18C-F ₆ -BZ-H ₄ -Fe | -0.339 | -1.214 | -0.199 | 0.140 | -0.393 | 19.61 |
| 18B-W ₄ -BZ-H ₄ -Fe | -0.773 | -1.241 | -0.582 | 0.191 | -0.474 | 22.68 |
| 18C-W ₄ -BZ-H ₄ -Fe | -0.337 | -1.221 | -0.201 | 0.136 | -0.406 | 19.72 |

Table S - 14. Orbital energy differences used to correlate electronics with reactivity, all values listed in eV. $\Delta E_{H(\alpha)-L(\alpha)}$ is the HOMO-LUMO gap for α orbitals, $\Delta E_{H(\beta)-L(\beta)}$ is the HOMO-LUMO gap for the β molecular orbitals. The $\Delta E_{\sigma^*(\alpha)-\pi^*(\beta)}$ column represents the two “competing” orbitals in radical formation, the α -d_{z² orbital and the β -d_{xz}, and the last column contains the activation barrier for the formation of the radical intermediate (TS2) ($\Delta G_{\text{Act}}^\ddagger$ values in kcal/mol).}

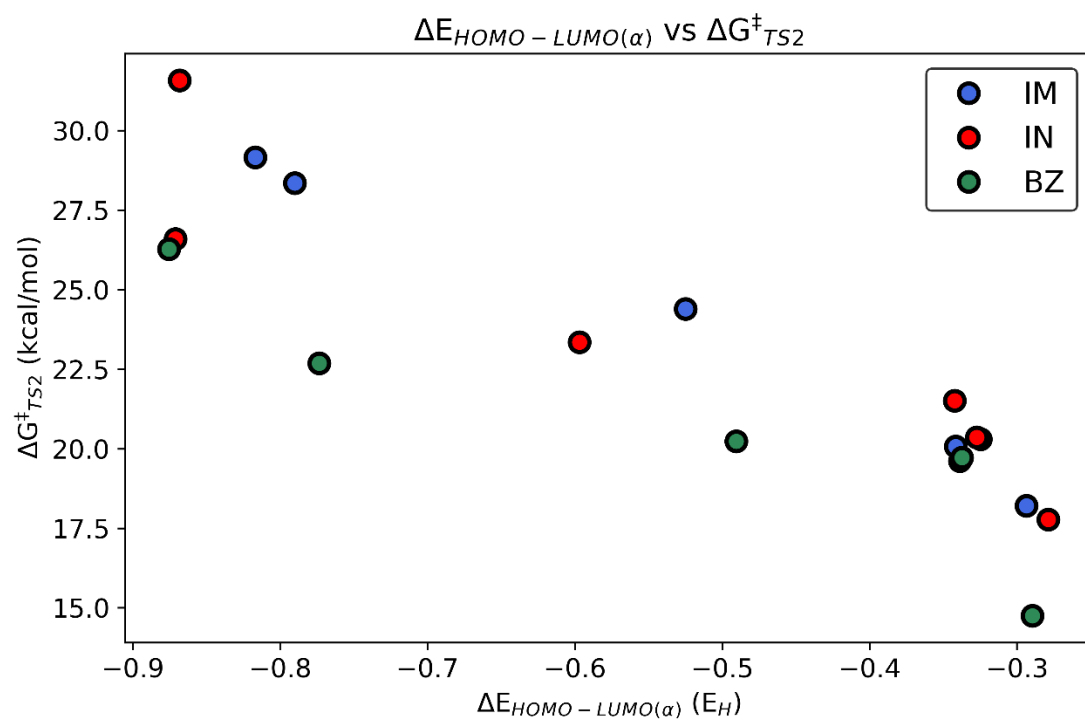


Figure S - 6. Scatter plot of the HOMO-LUMO gap of α molecular orbitals, orbital energies displayed in Hartree and activation barriers are presented in kcal/mol. The data points are

separated based on the NHC subunits, imidazoles (IM) shown in blue, imidazolines (IN) shown in red and benzimidazoles (BZ) shown in green.

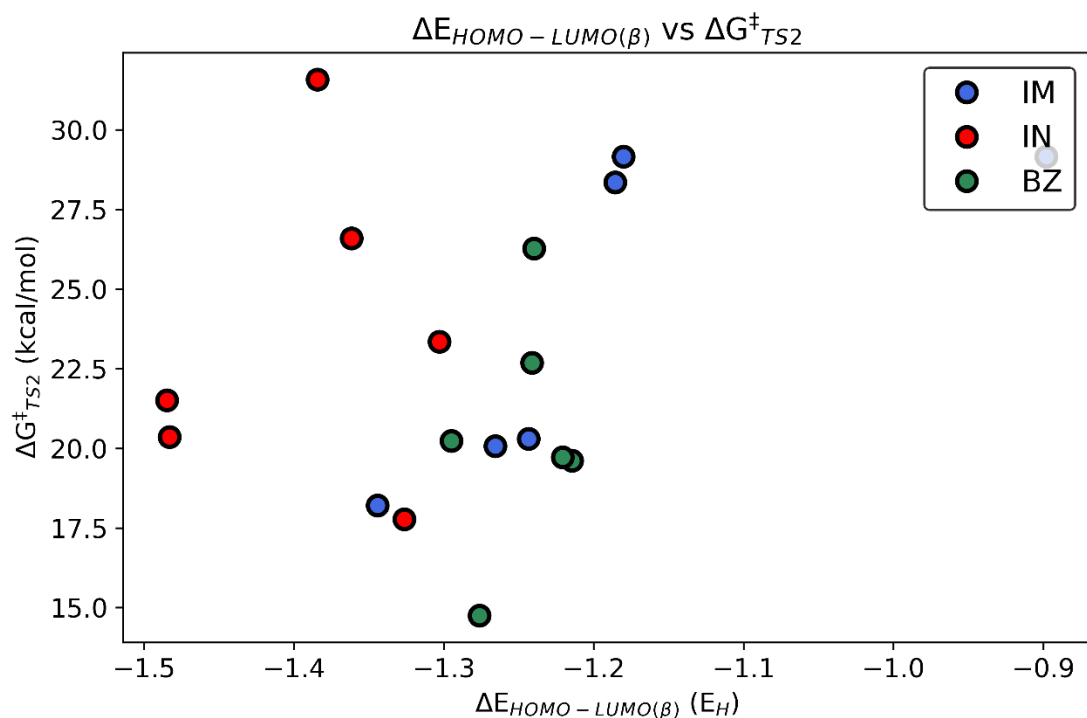


Figure S - 7. Scatter plot of the HOMO-LUMO gap of β molecular orbitals, orbital energies displayed in Hartree and activation barriers are presented in kcal/mol. The data points are

separated based on the NHC subunits, imidazoles (IM) shown in blue, imidazolines (IN) shown in red and benzimidazoles (BZ) shown in green.

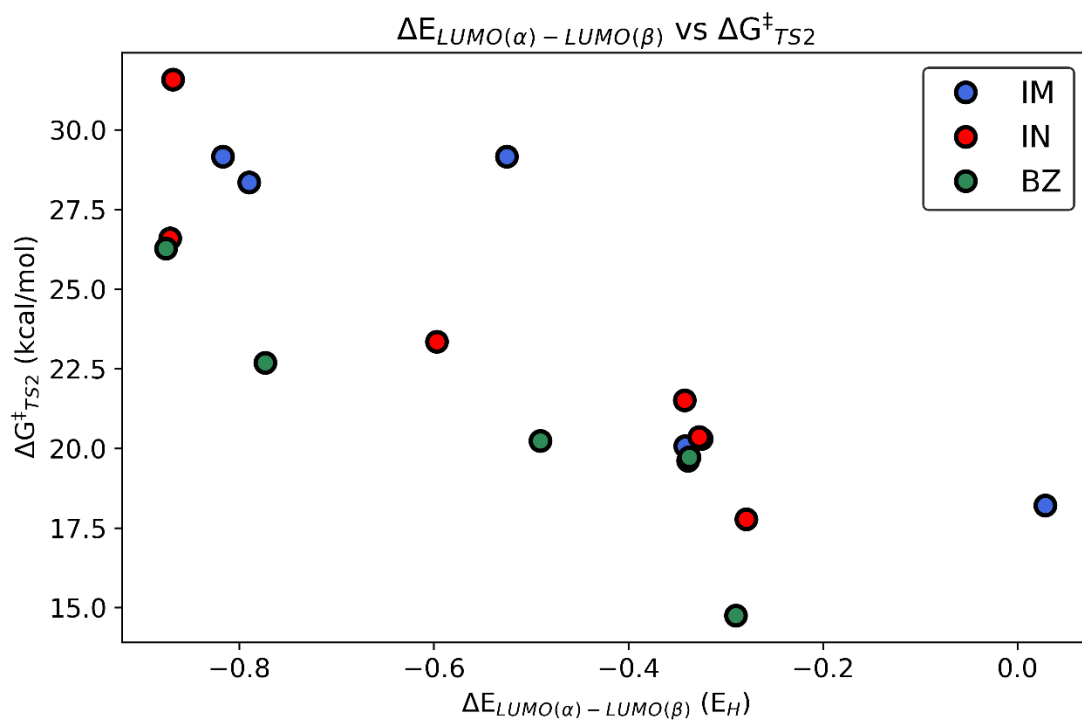


Figure S - 8. Scatter plot of the HOMO-LUMO gap of α and β molecular orbitals, orbital energies displayed in Hartree and activation barriers are presented in kcal/mol. In these cases, the HOMO is of α -spin and the LUMO is of β -spin. The data points are separated based on the NHC subunits, imidazoles (IM) shown in blue, imidazolines (IN) shown in red and benzimidazoles (BZ) shown in green.

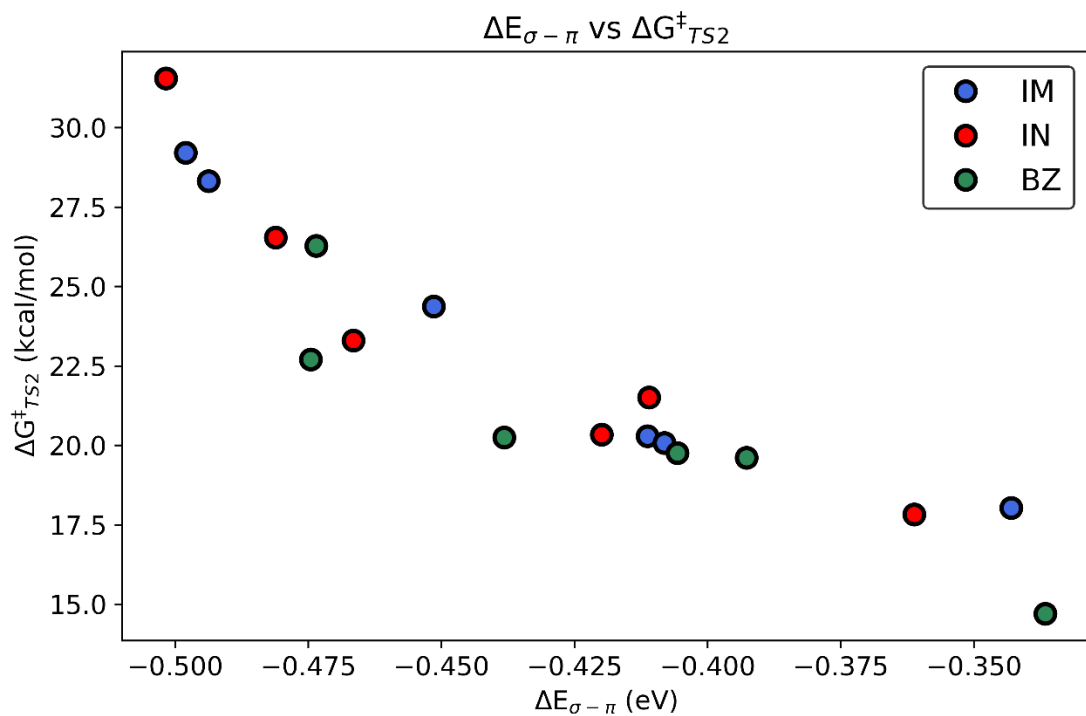
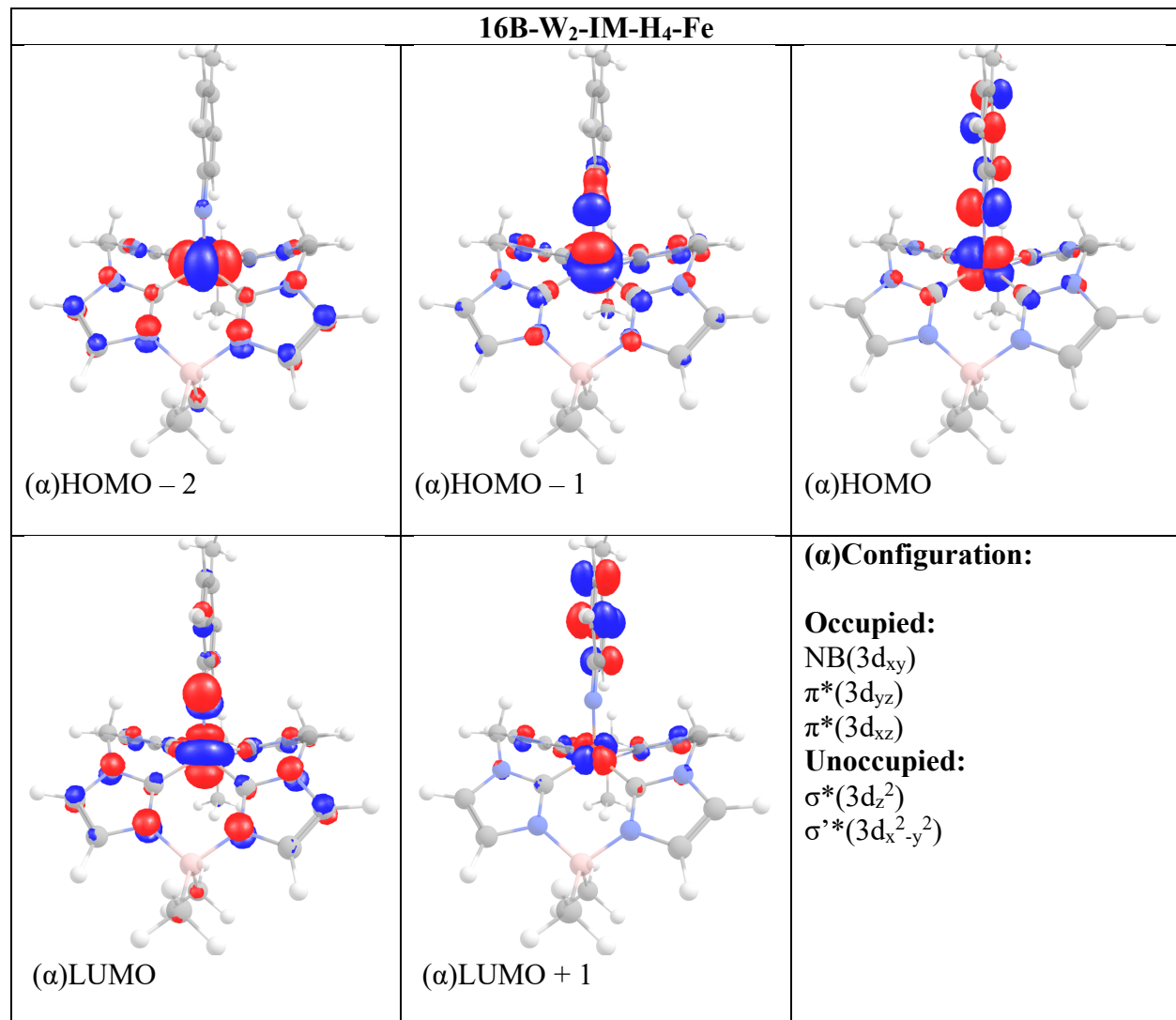
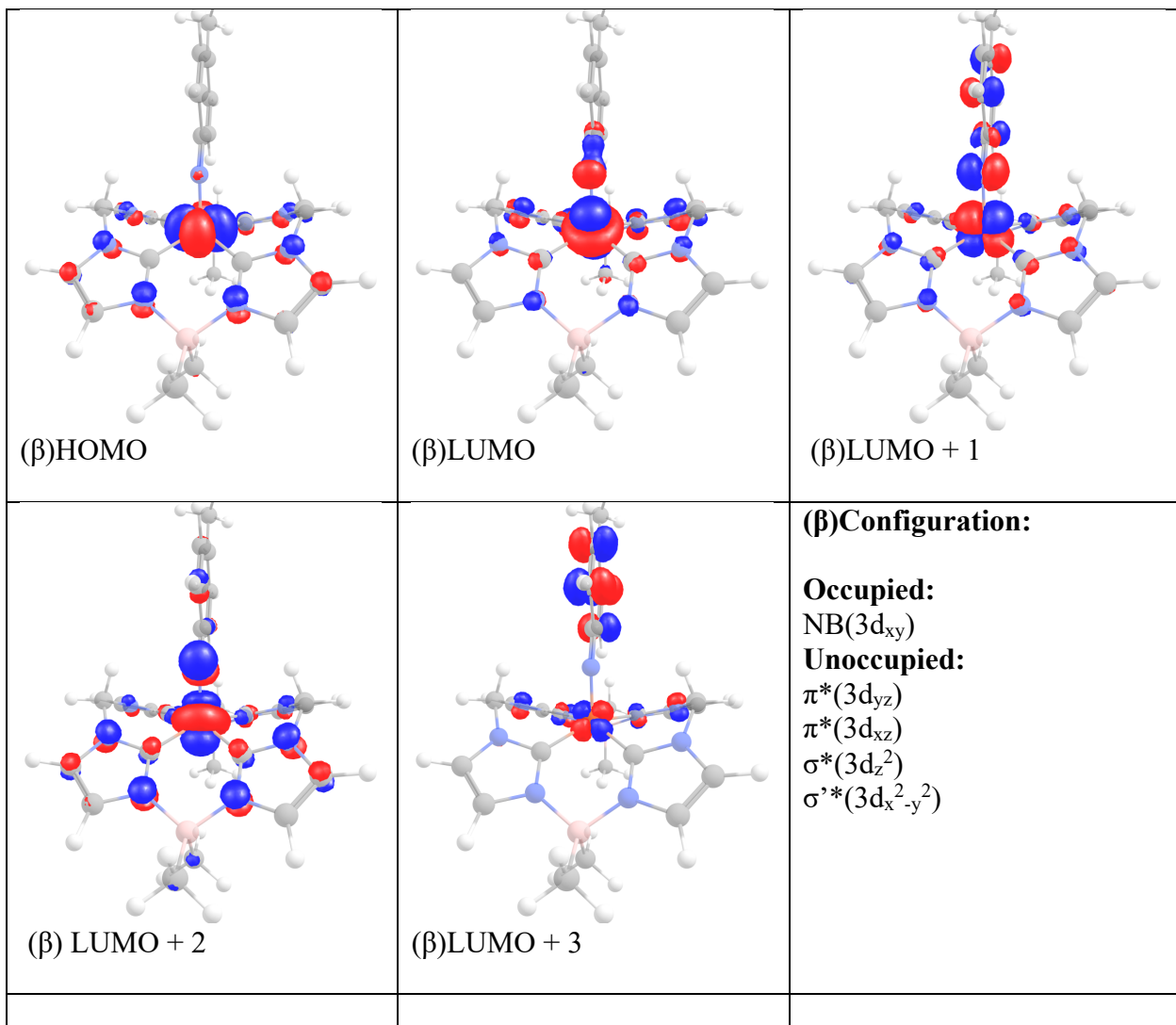


Figure S - 9. Scatter plot of the σ^* (d_{z^2}) orbital with α -spin subtracted from the π^* ($d_{xz/yz}$) orbital with β -spin. In the carbon-based complexes this is LUMO(α) and LUMO+1(β), and in the complexes linked with dimethyl borates this is LUMO(α) and LUMO+2(β). The data points are separated based on the NHC subunits, imidazoles (IM) shown in blue, imidazolines (IN) shown in red and benzimidazoles (BZ) shown in green.

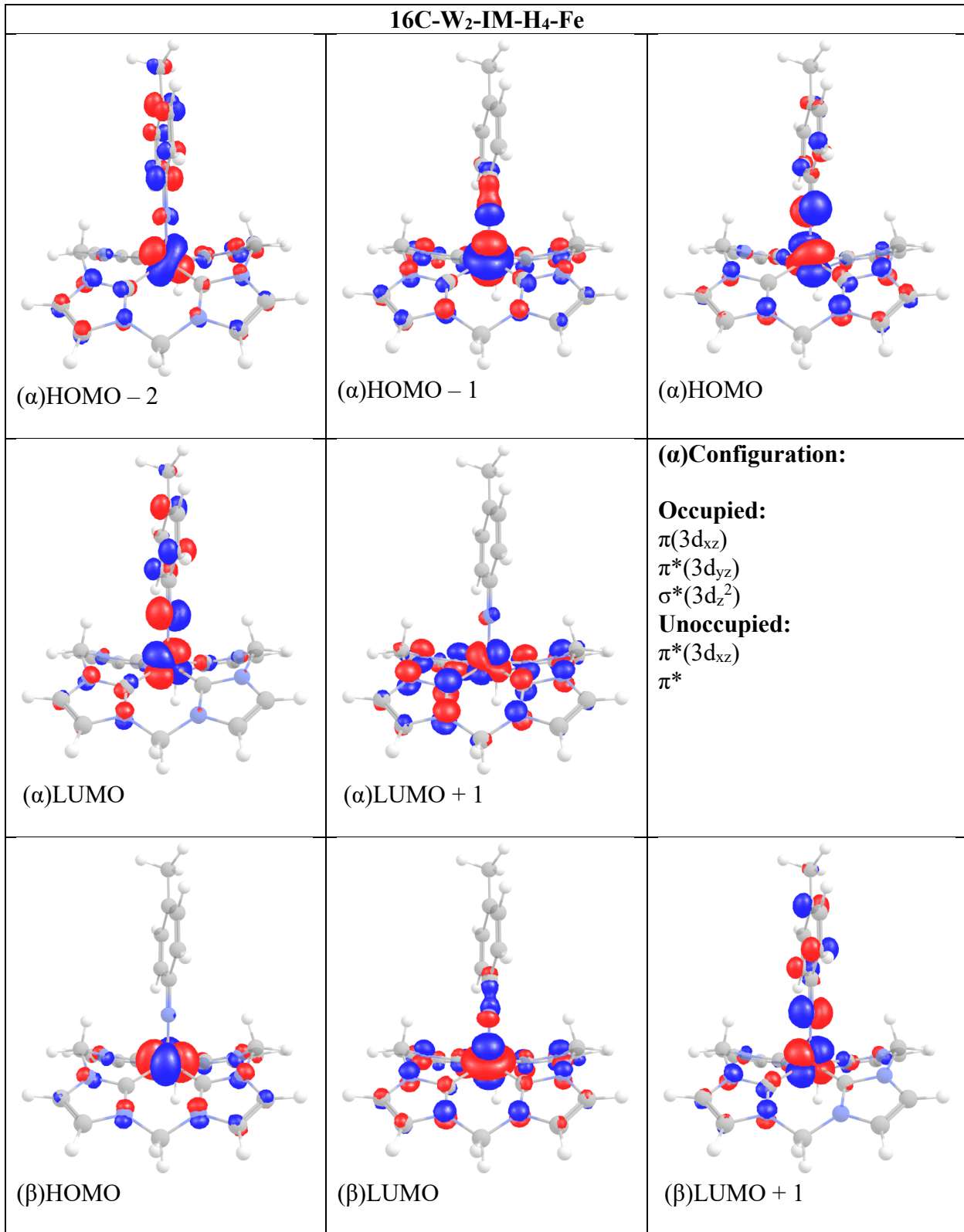
Section S3.1. Molecular Orbital Visualization and Selected Spin Densities

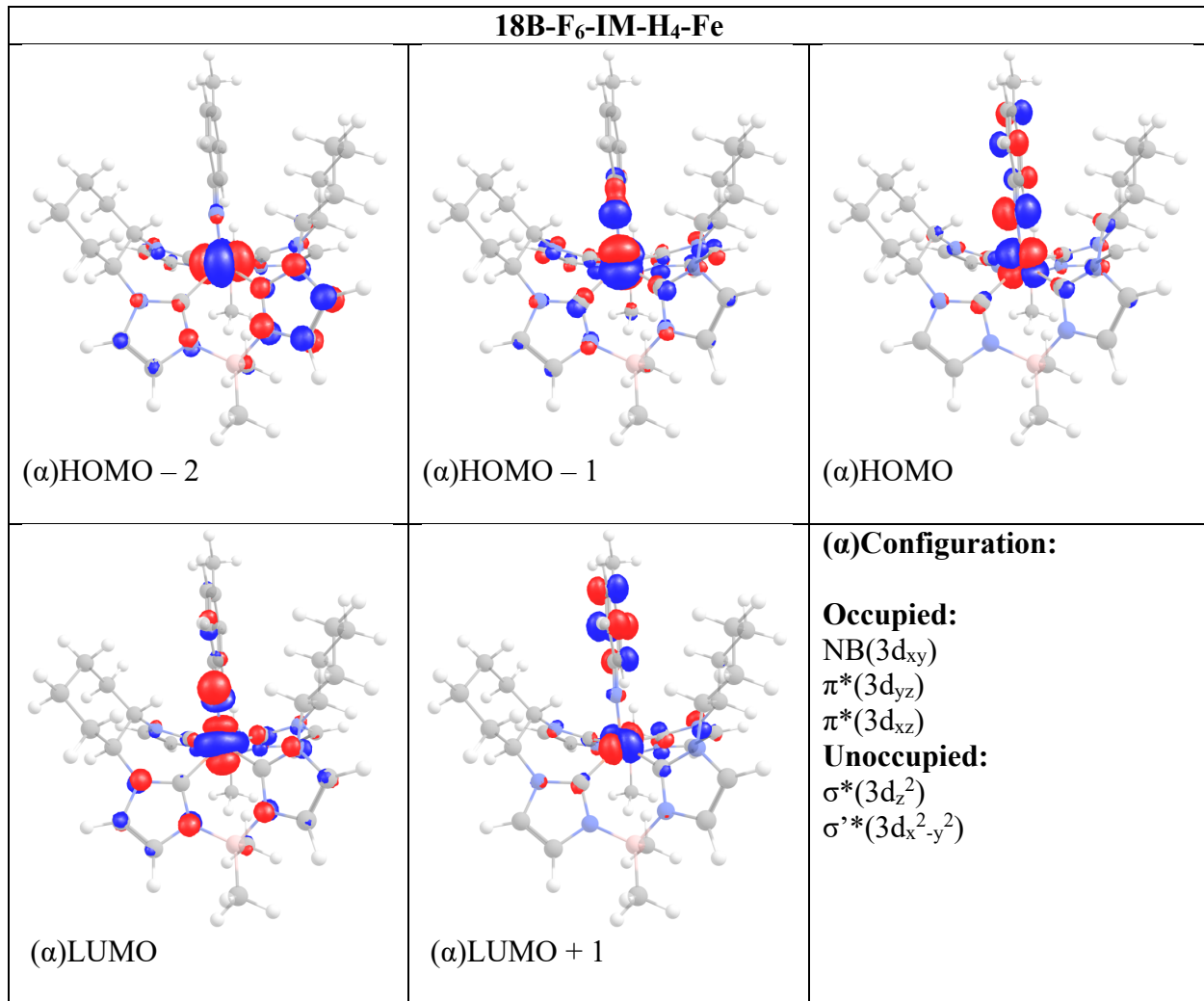
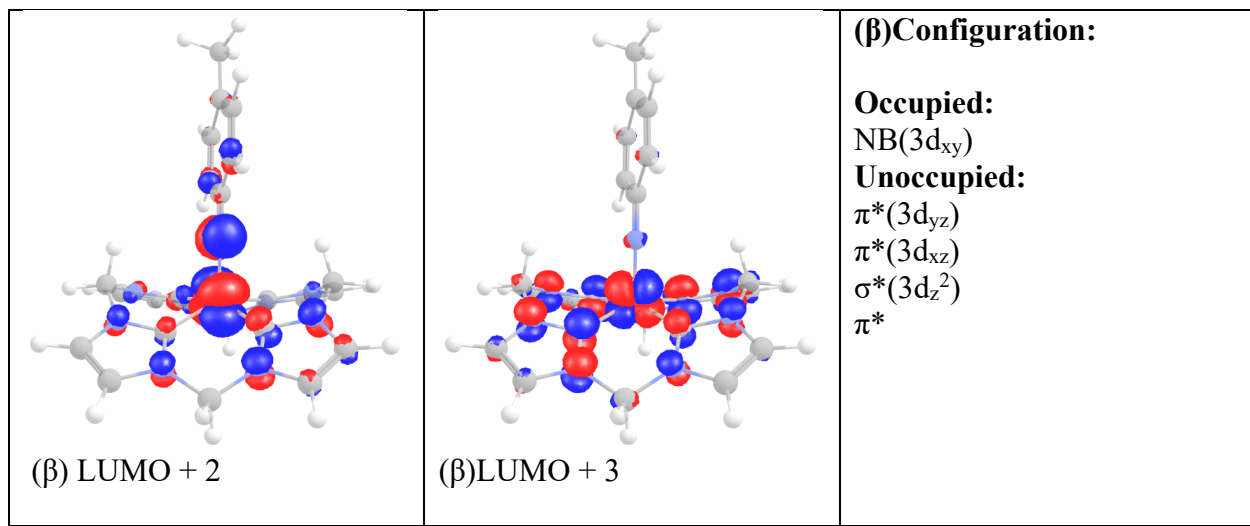
Frontier molecular orbitals of each iron(IV)-imide species. For α -spin orbitals this is the HOMO-2 up to LUMO+1, and for the β -spin orbitals this is HOMO up to the LUMO+3. All isosurfaces have been rendered at an isovalue of 0.08

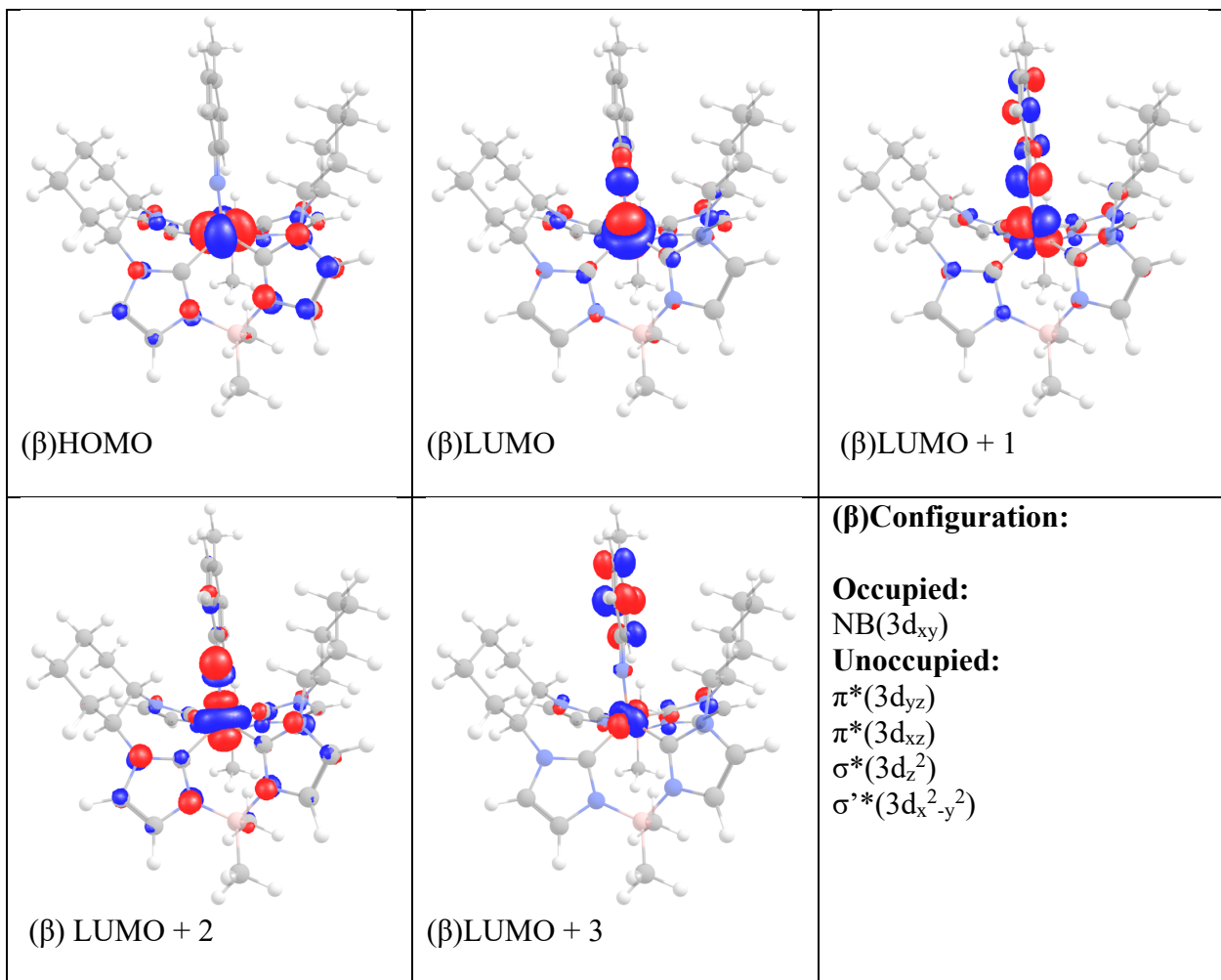




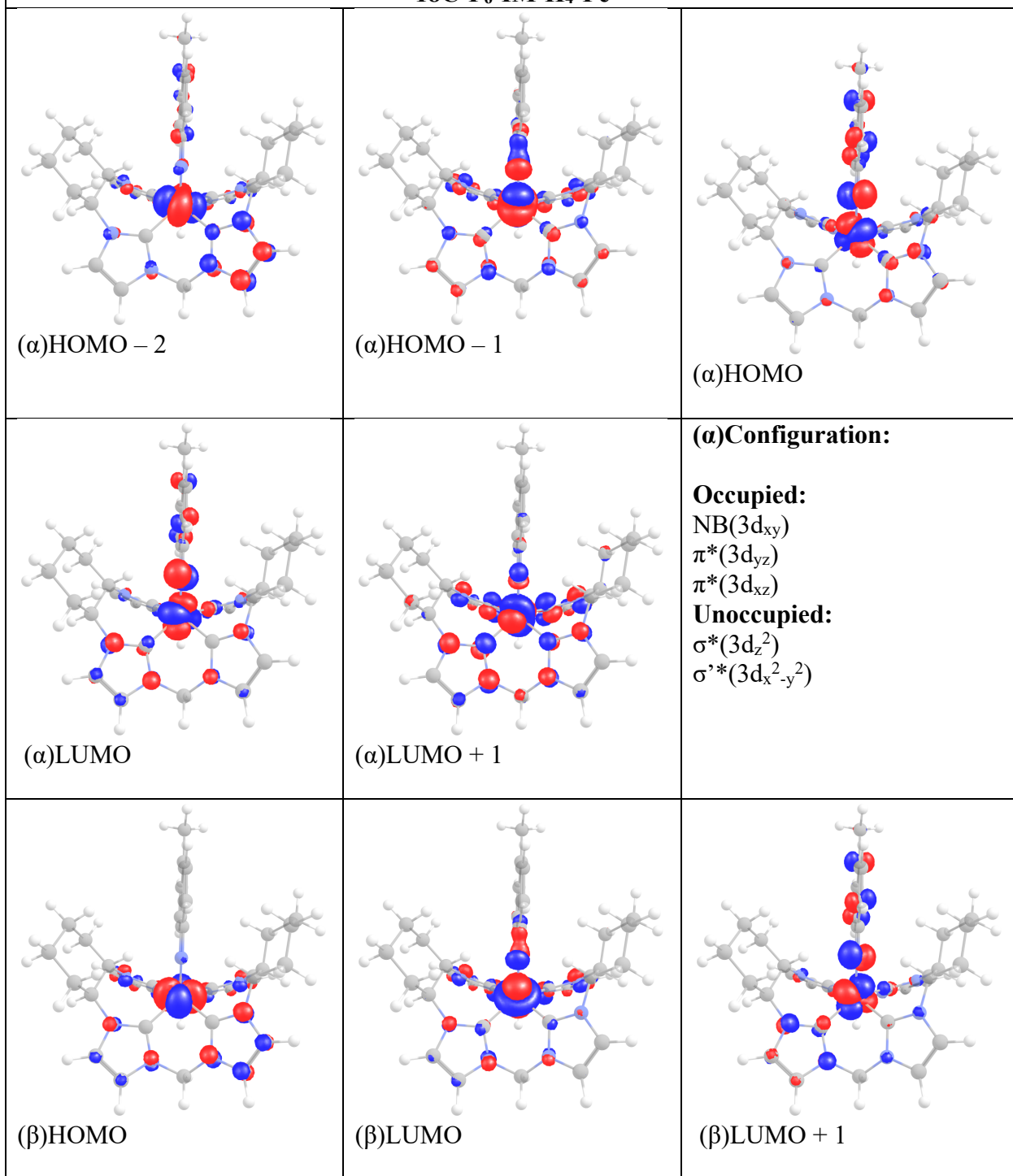
16C-W₂-IM-H₄-Fe

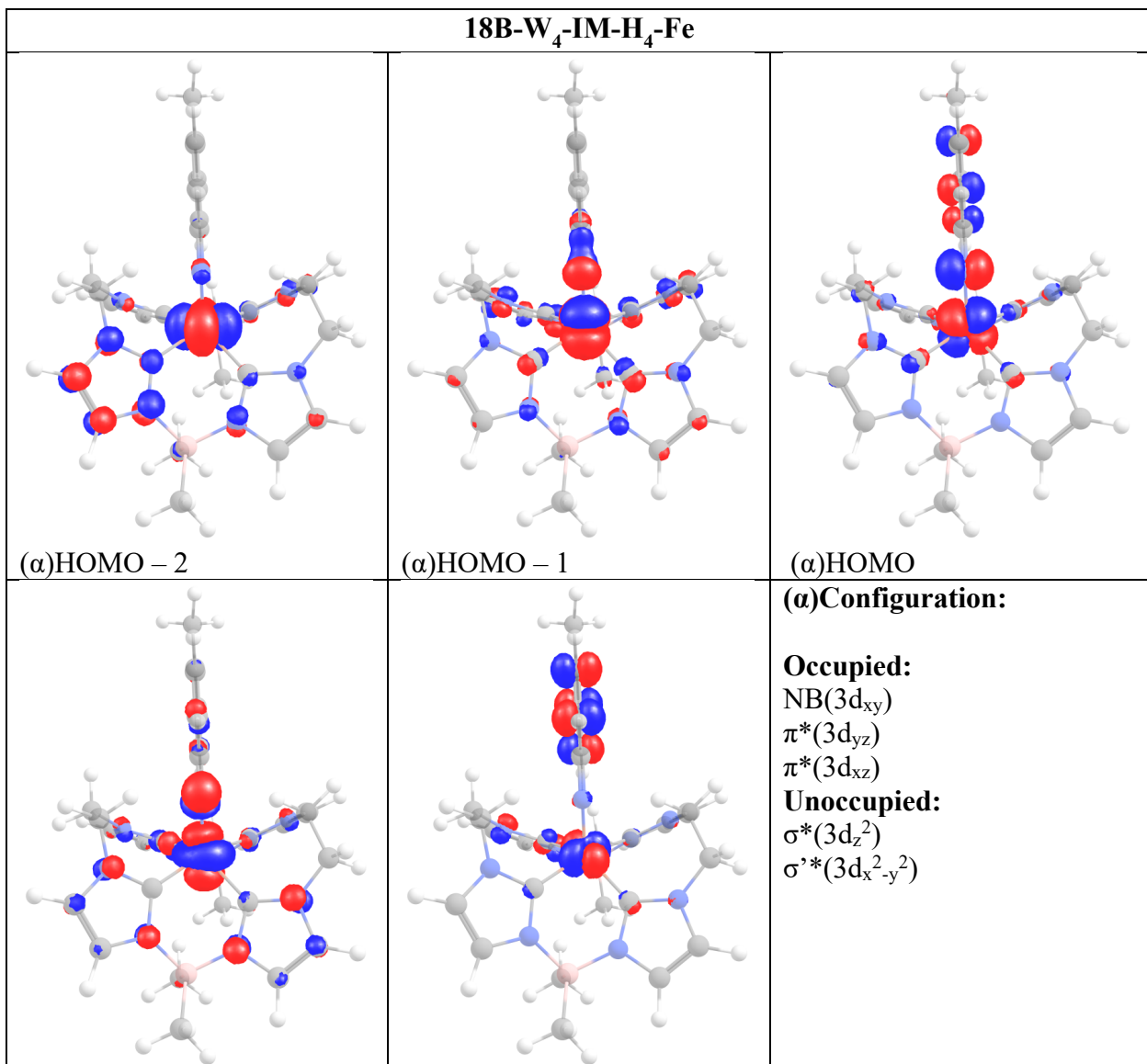
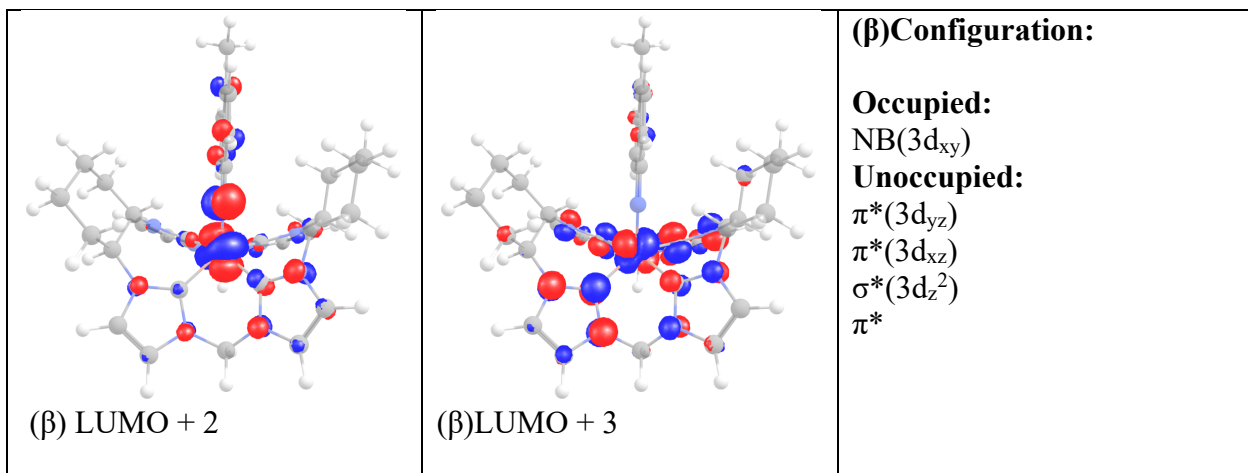


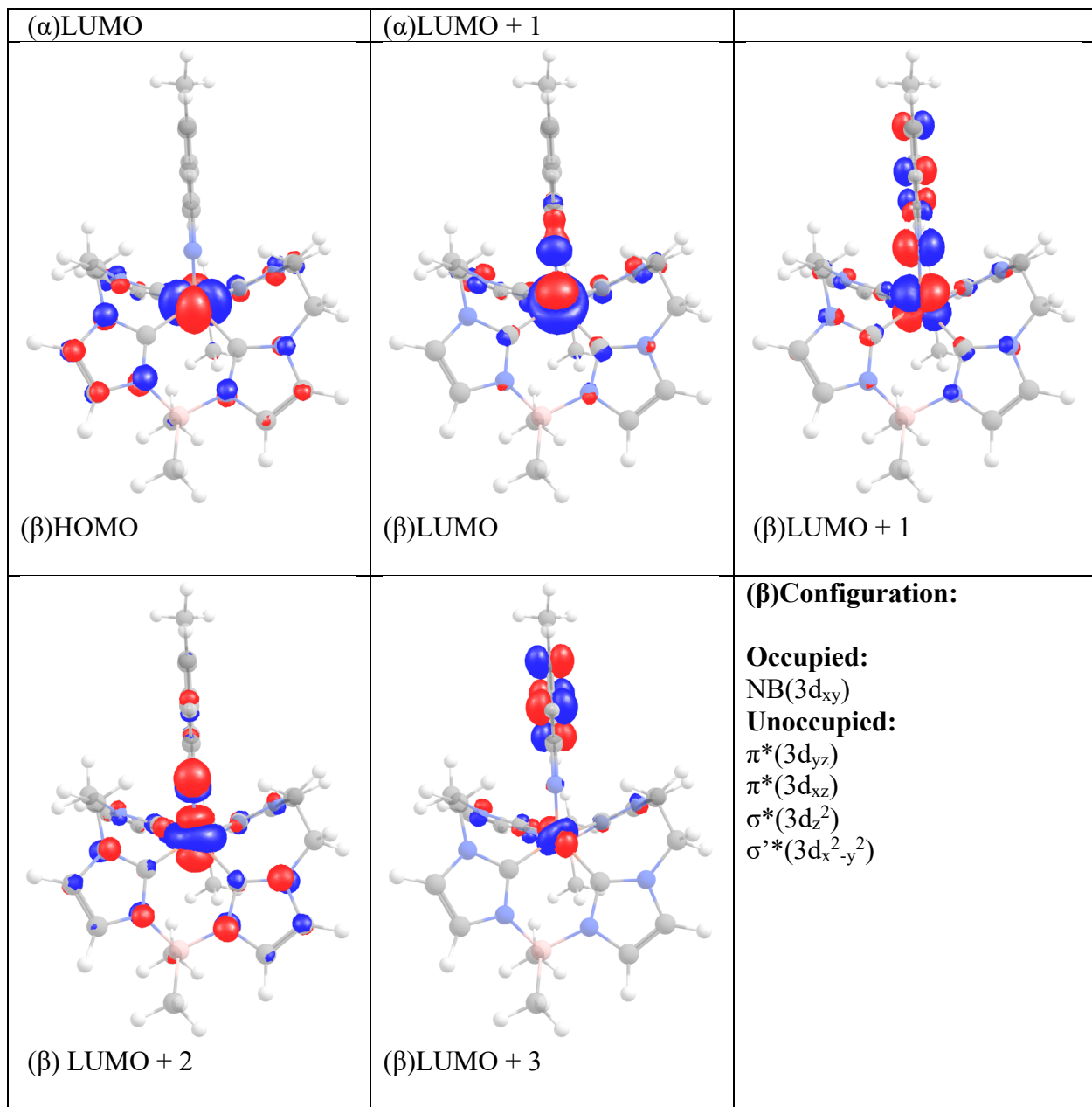


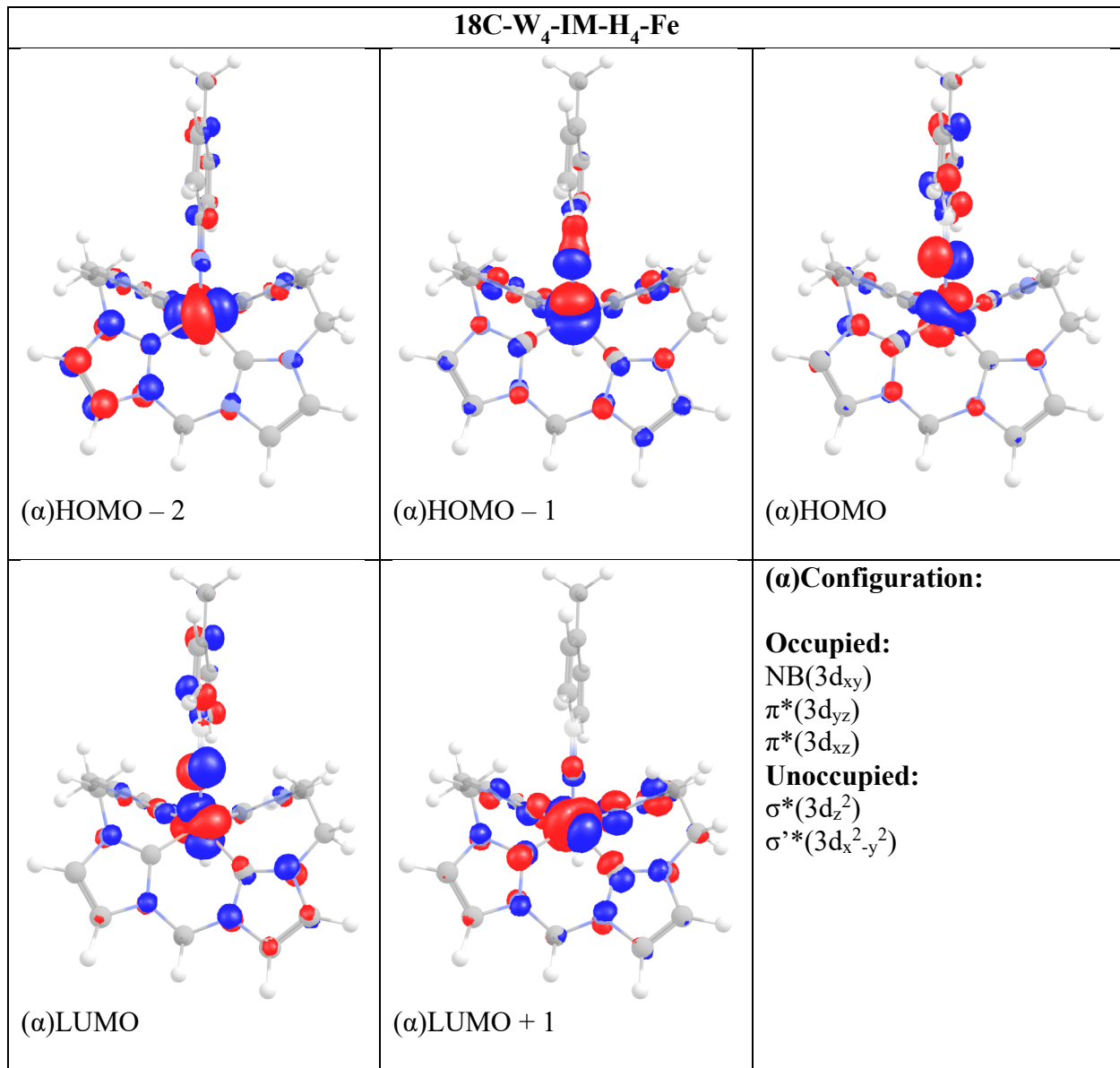


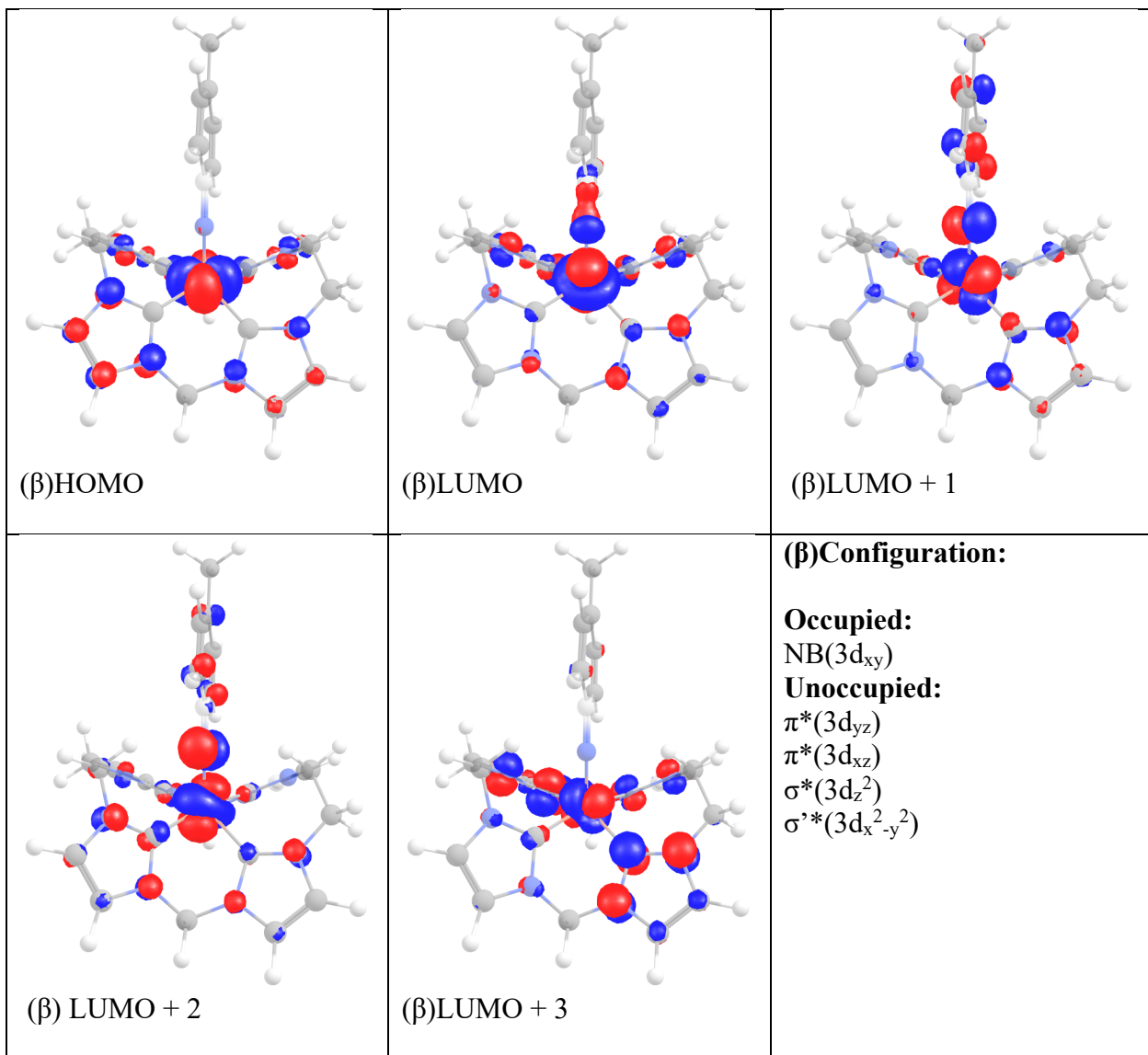
18C-F₆-IM-H₄-Fe



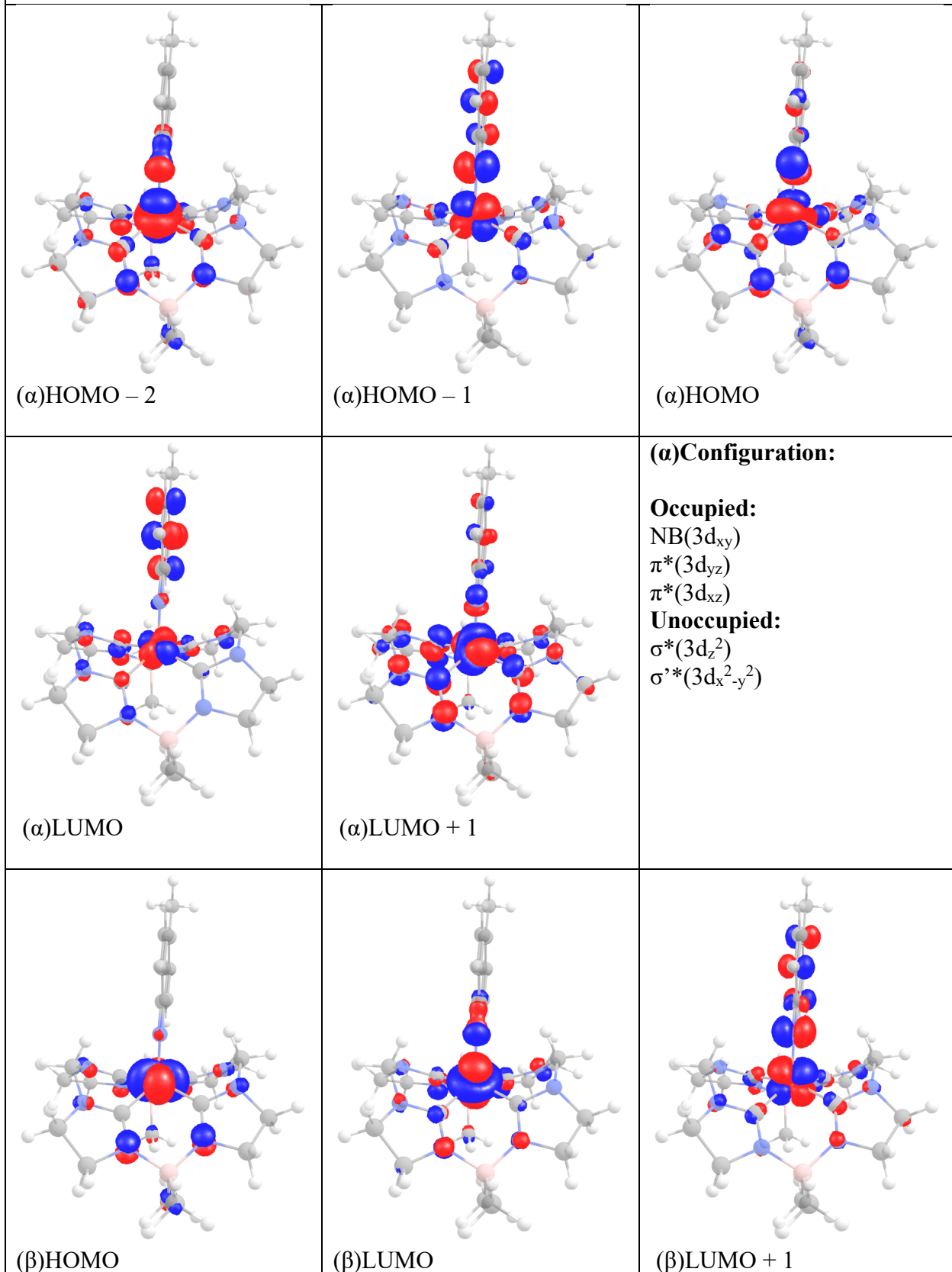


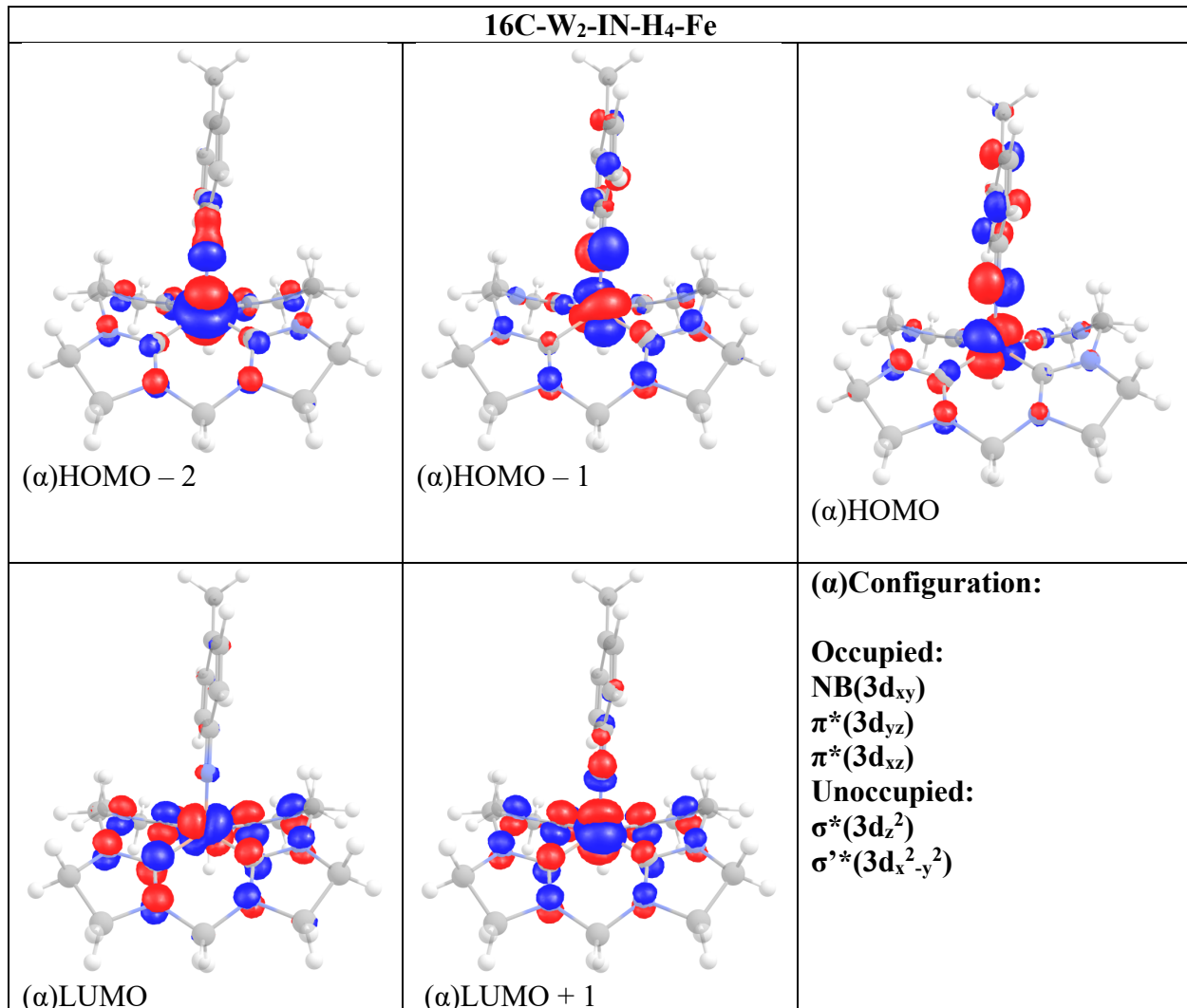
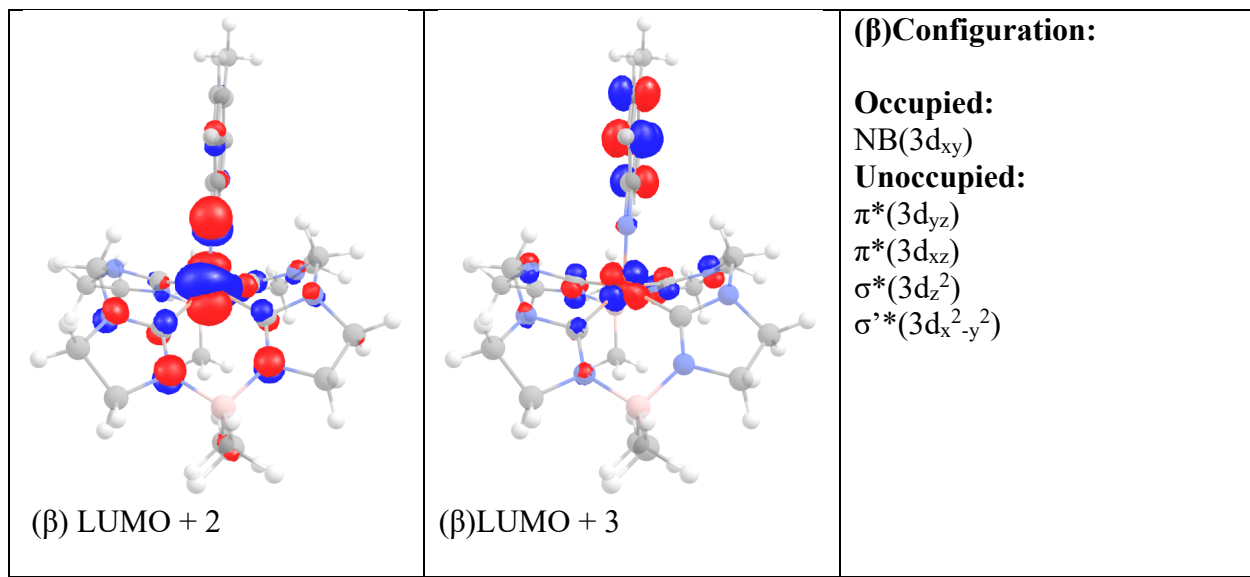


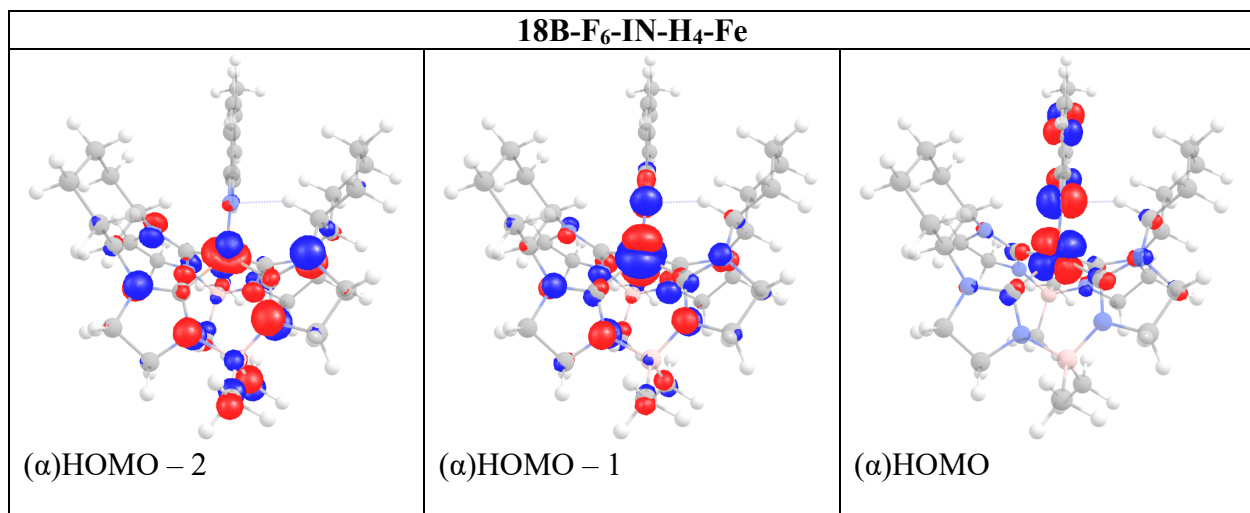
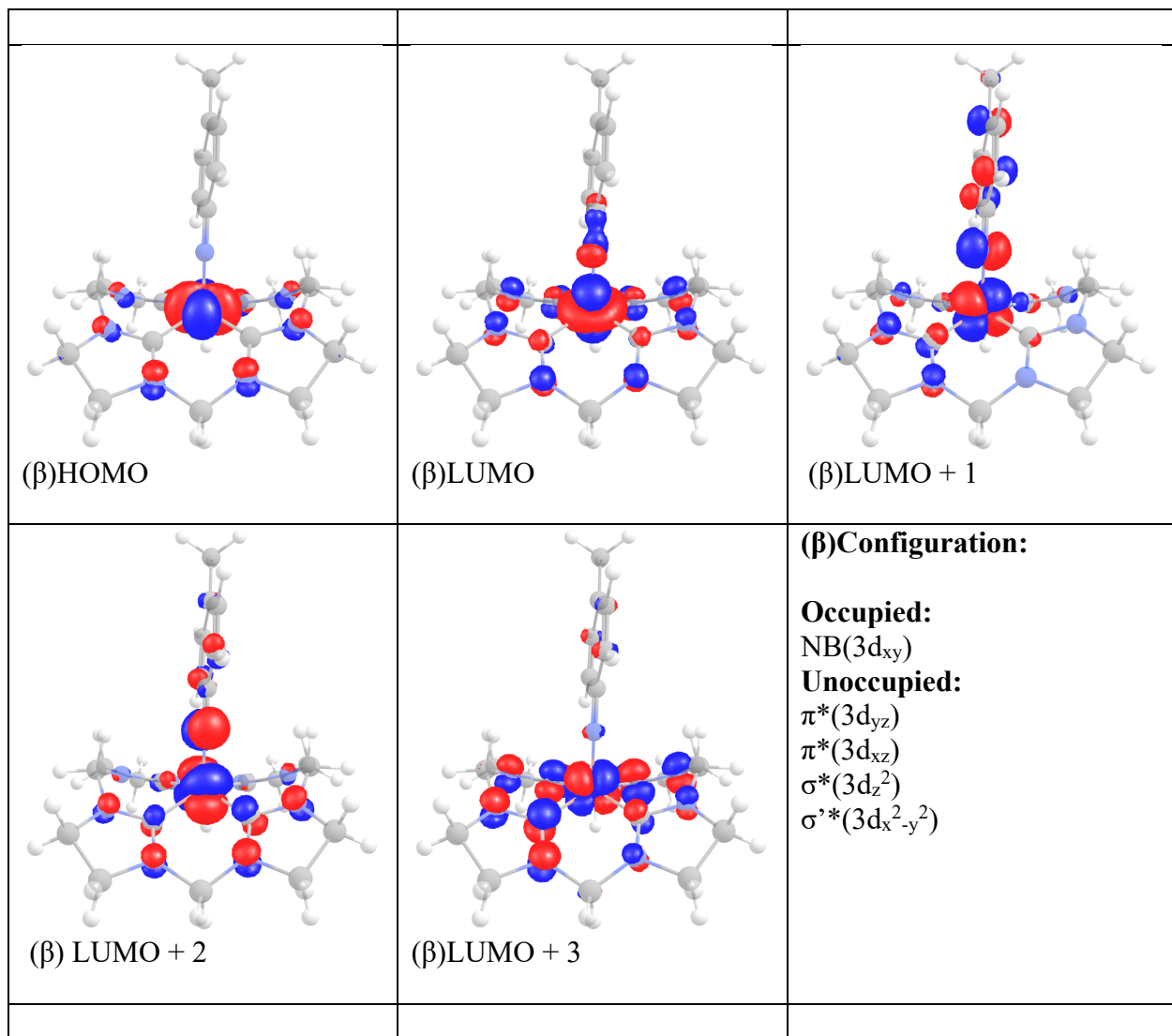


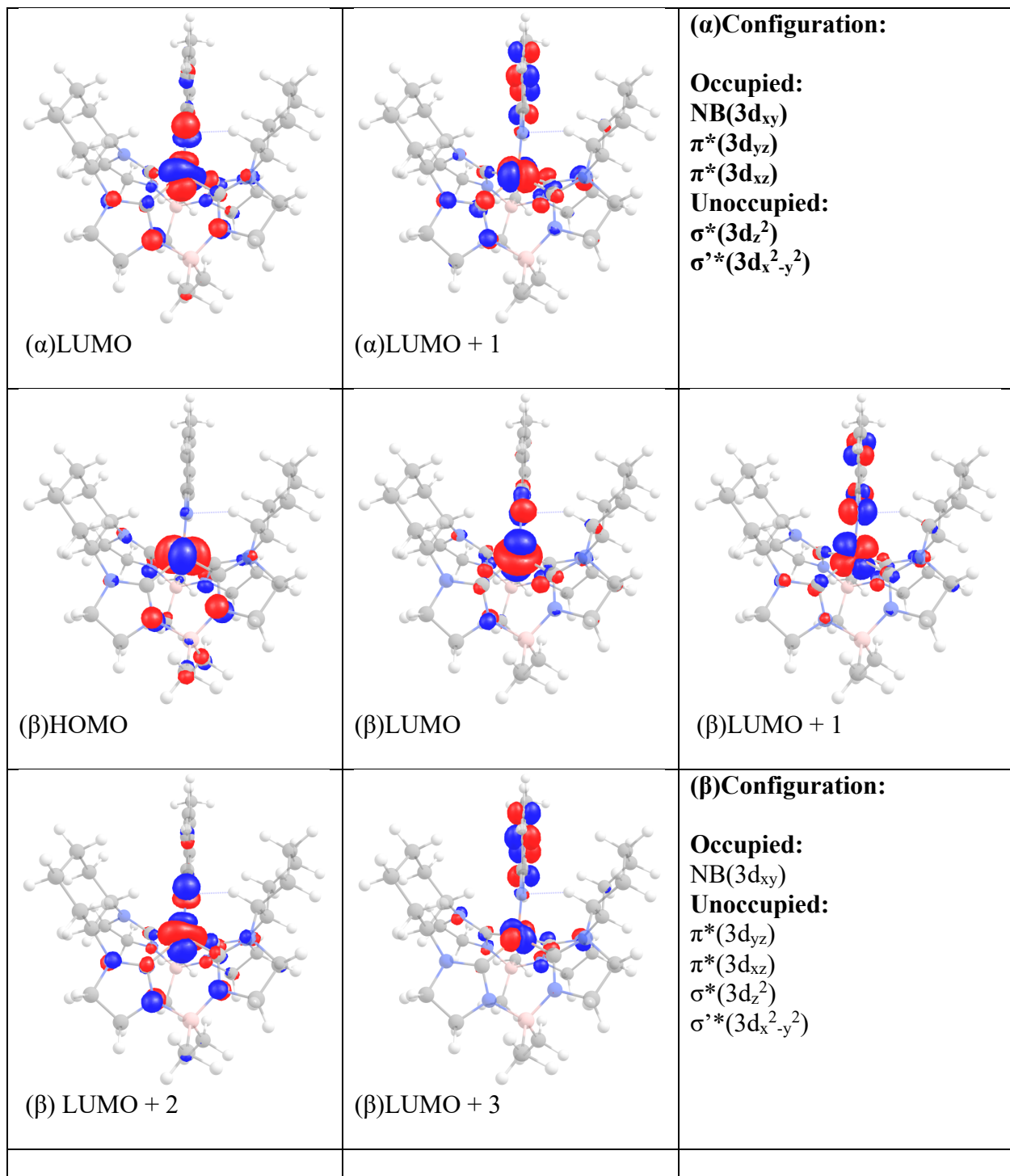


16B-W₂-IN-H₄-Fe

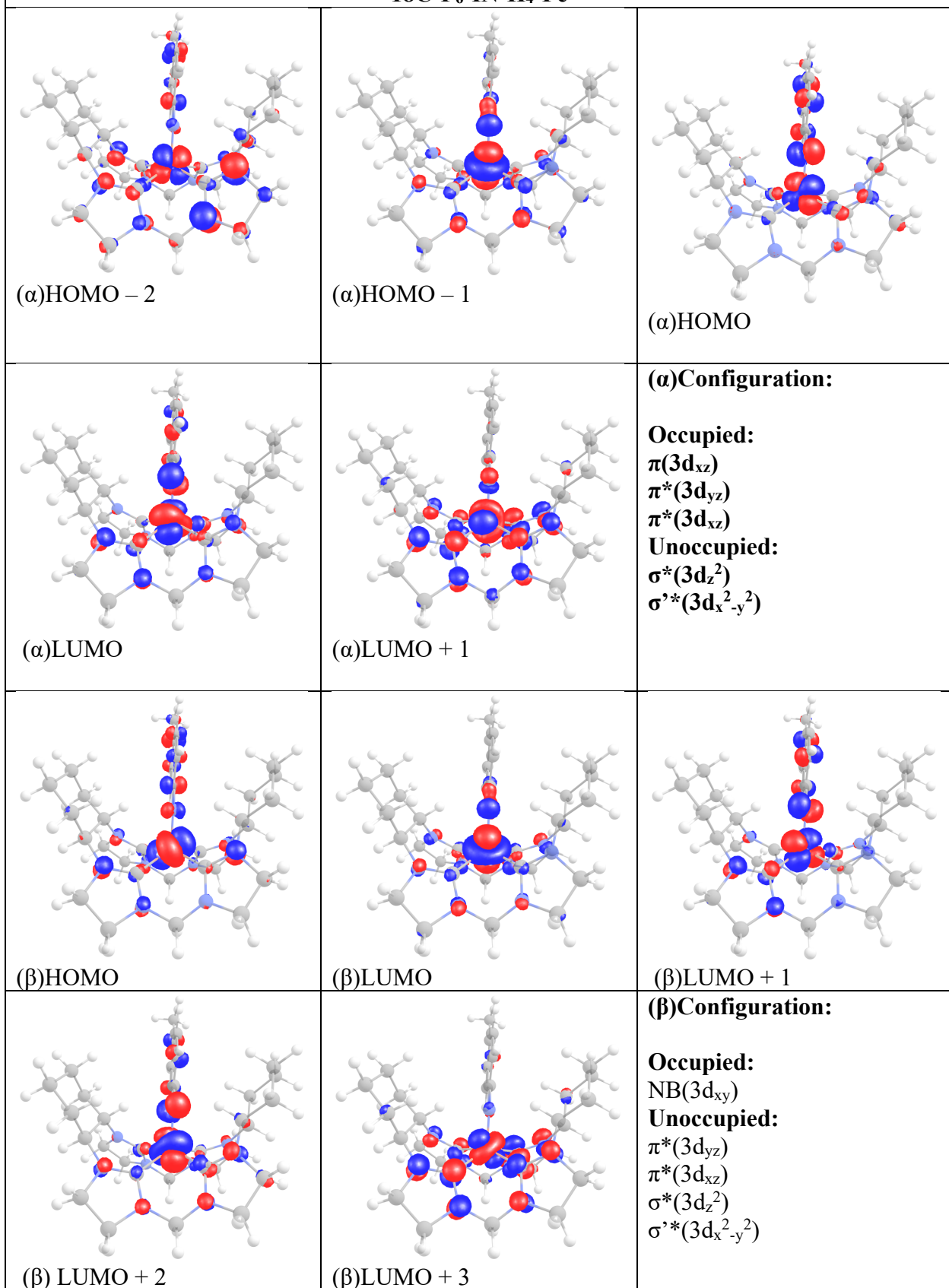




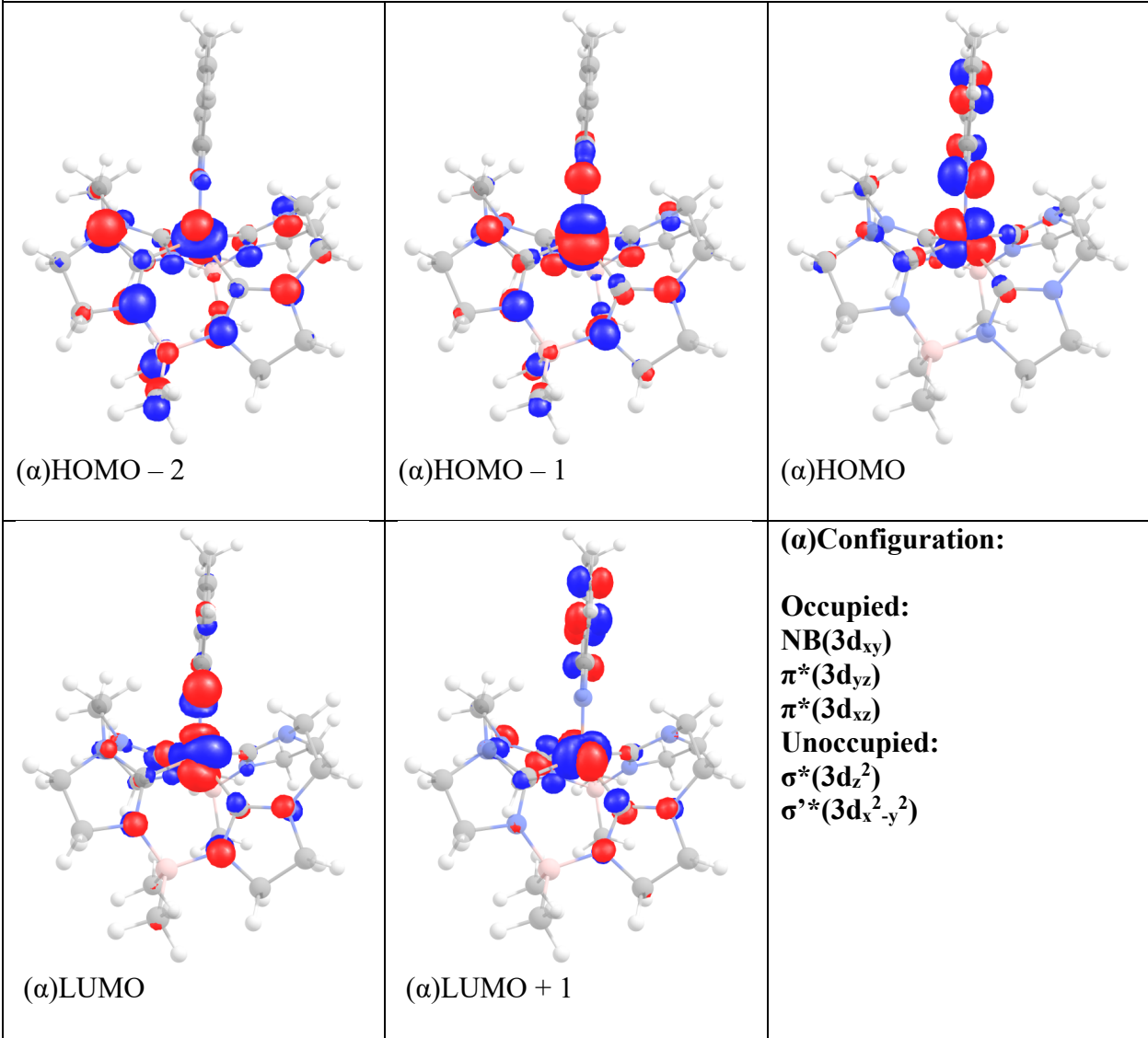


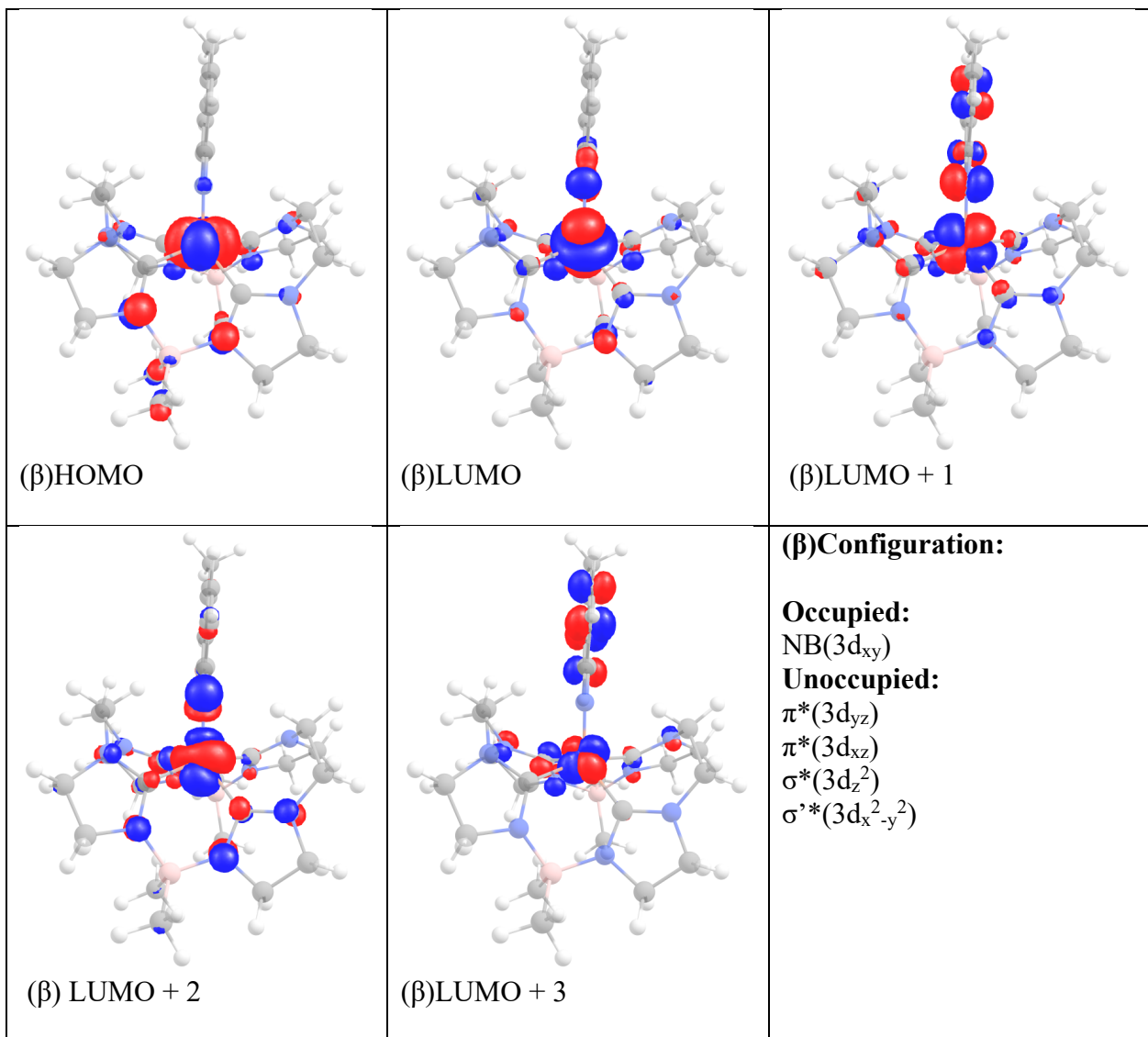


18C-F₆-IN-H₄-Fe

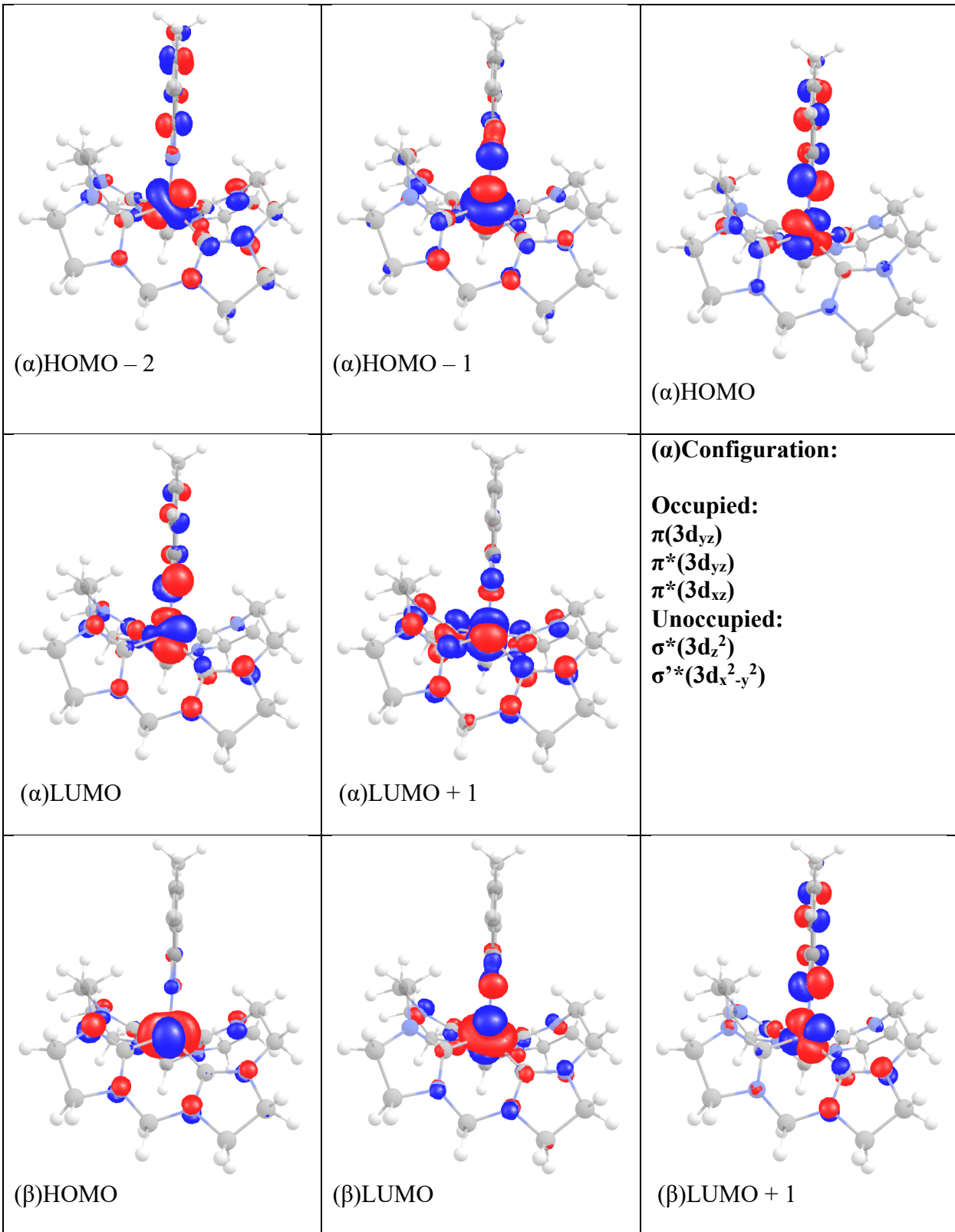


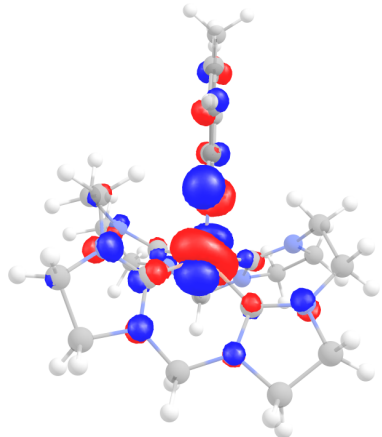
18B-W₄-IN-H₄-Fe



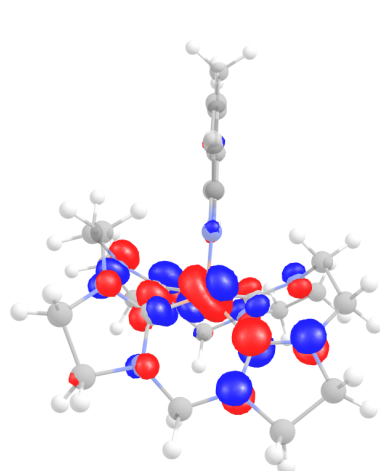


18C-W₄-IN-H₄-Fe





(β) LUMO + 2



(β) LUMO + 3

(β) Configuration:

Occupied:

NB($3d_{xy}$)

Unoccupied:

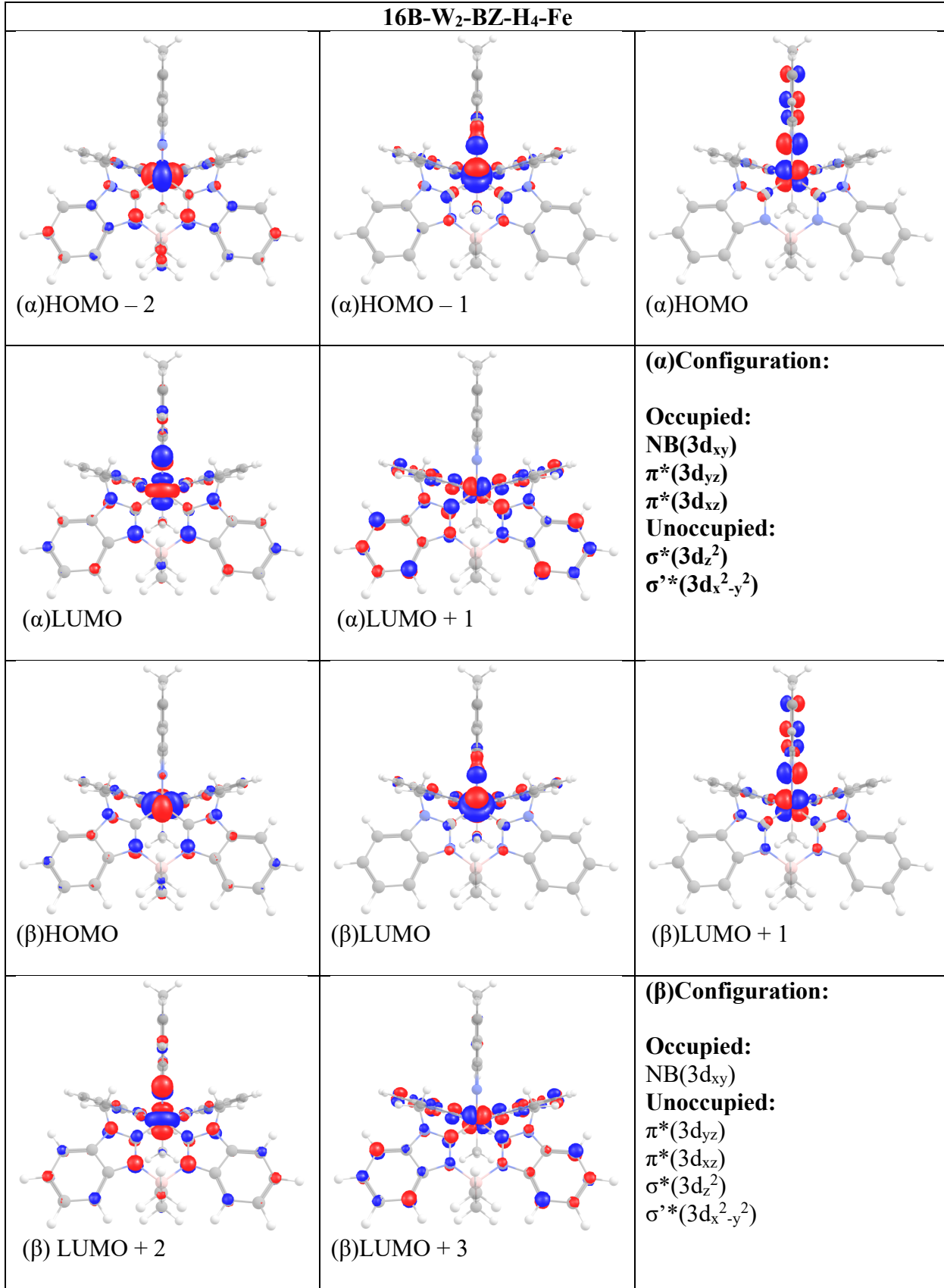
$\pi^*(3d_{yz})$

$\pi^*(3d_{xz})$

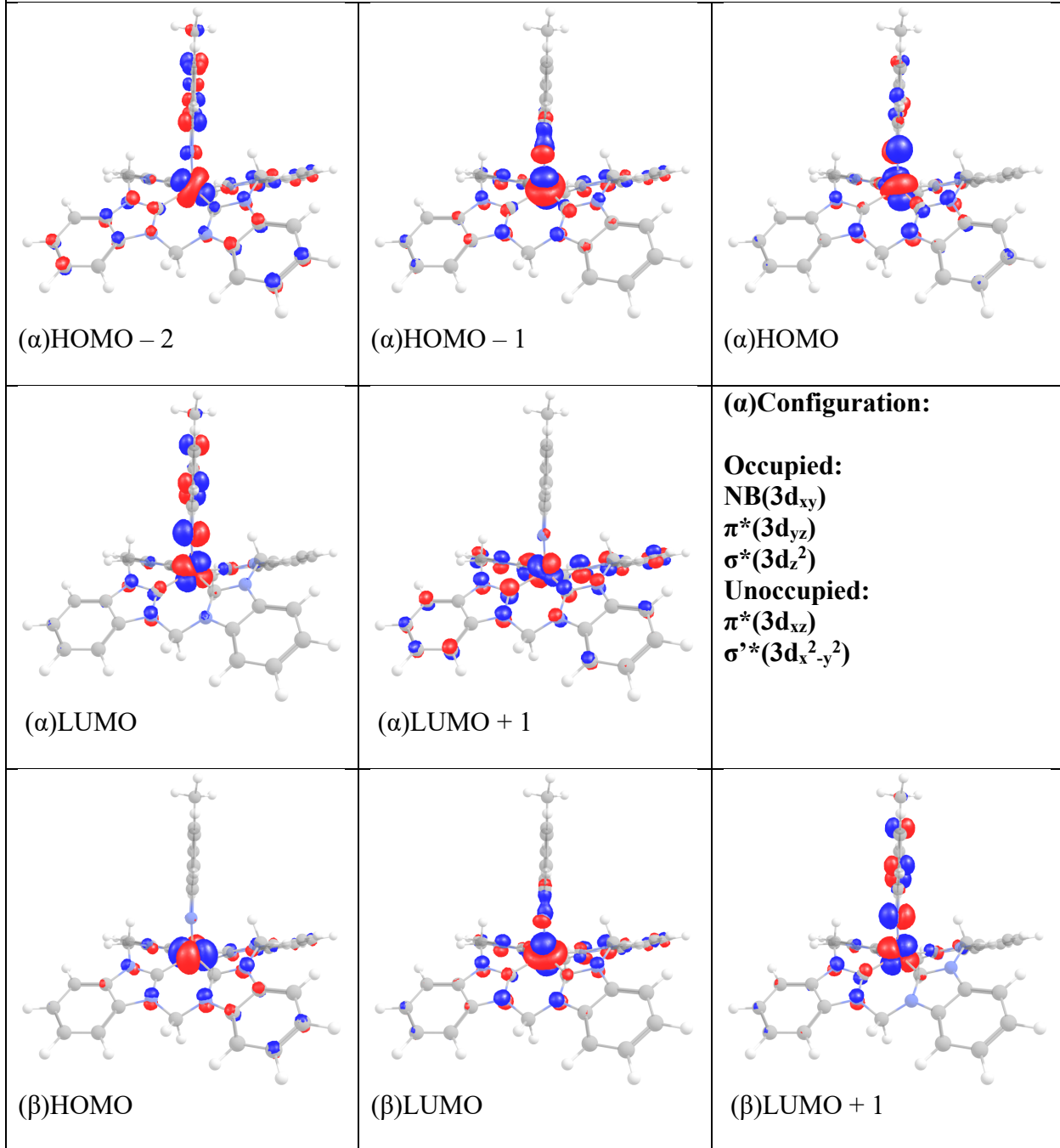
$\sigma^*(3d_z^2)$

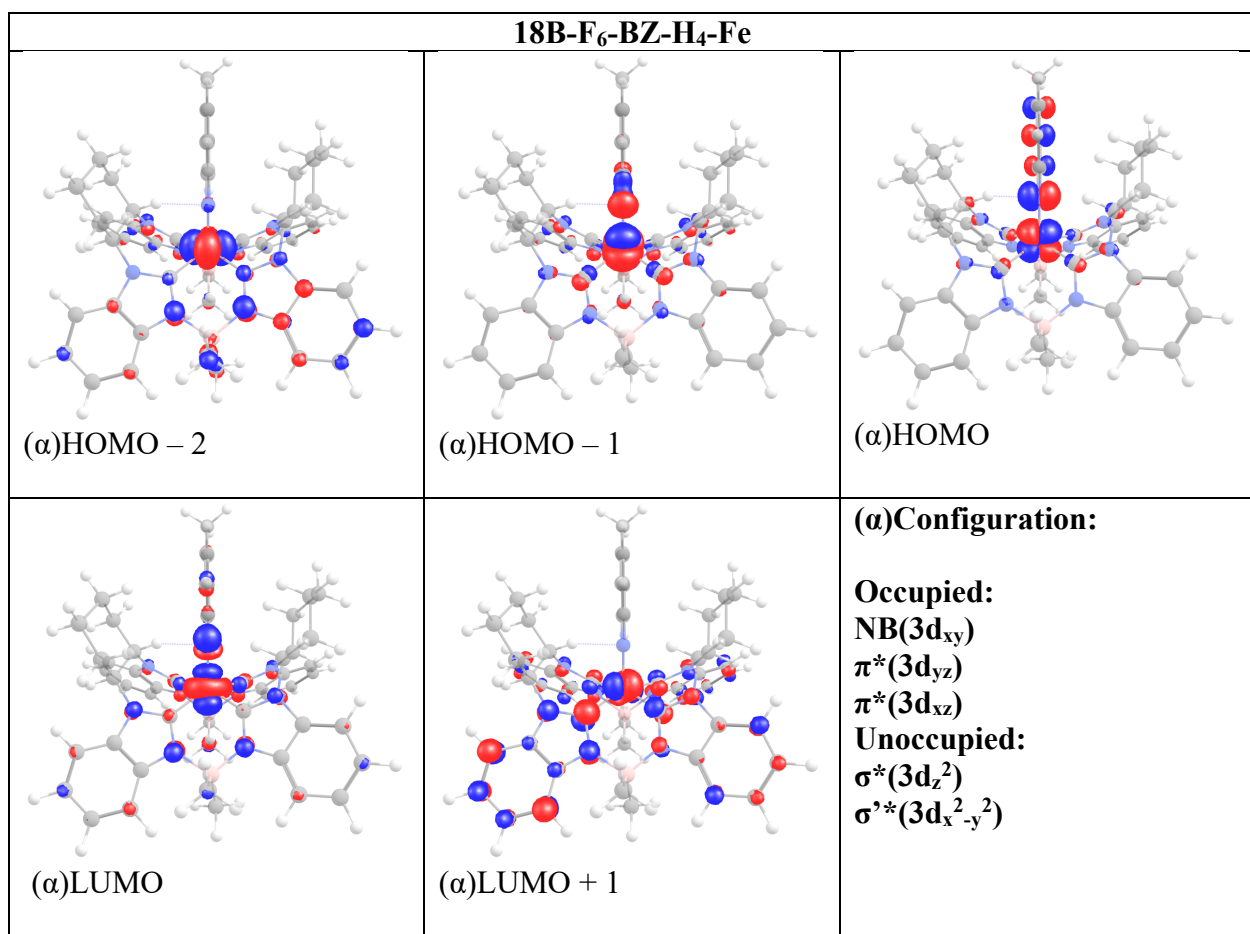
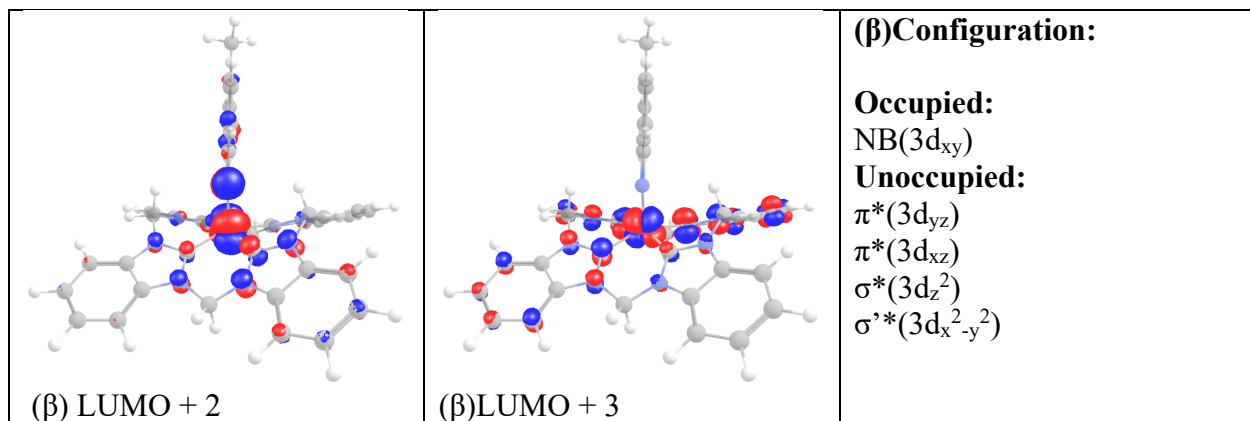
$\sigma'^*(3d_x^2 -)$

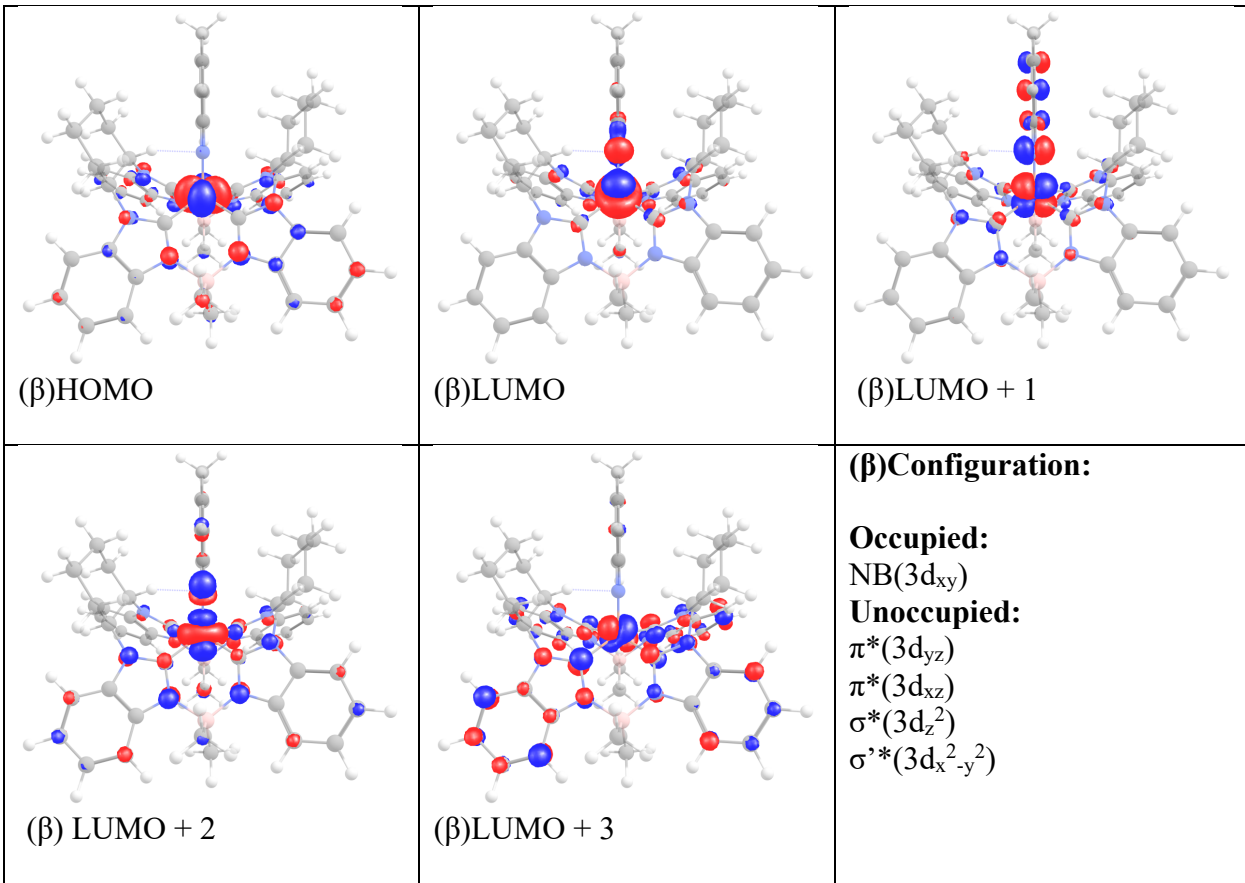
16B-W₂-BZ-H₄-Fe



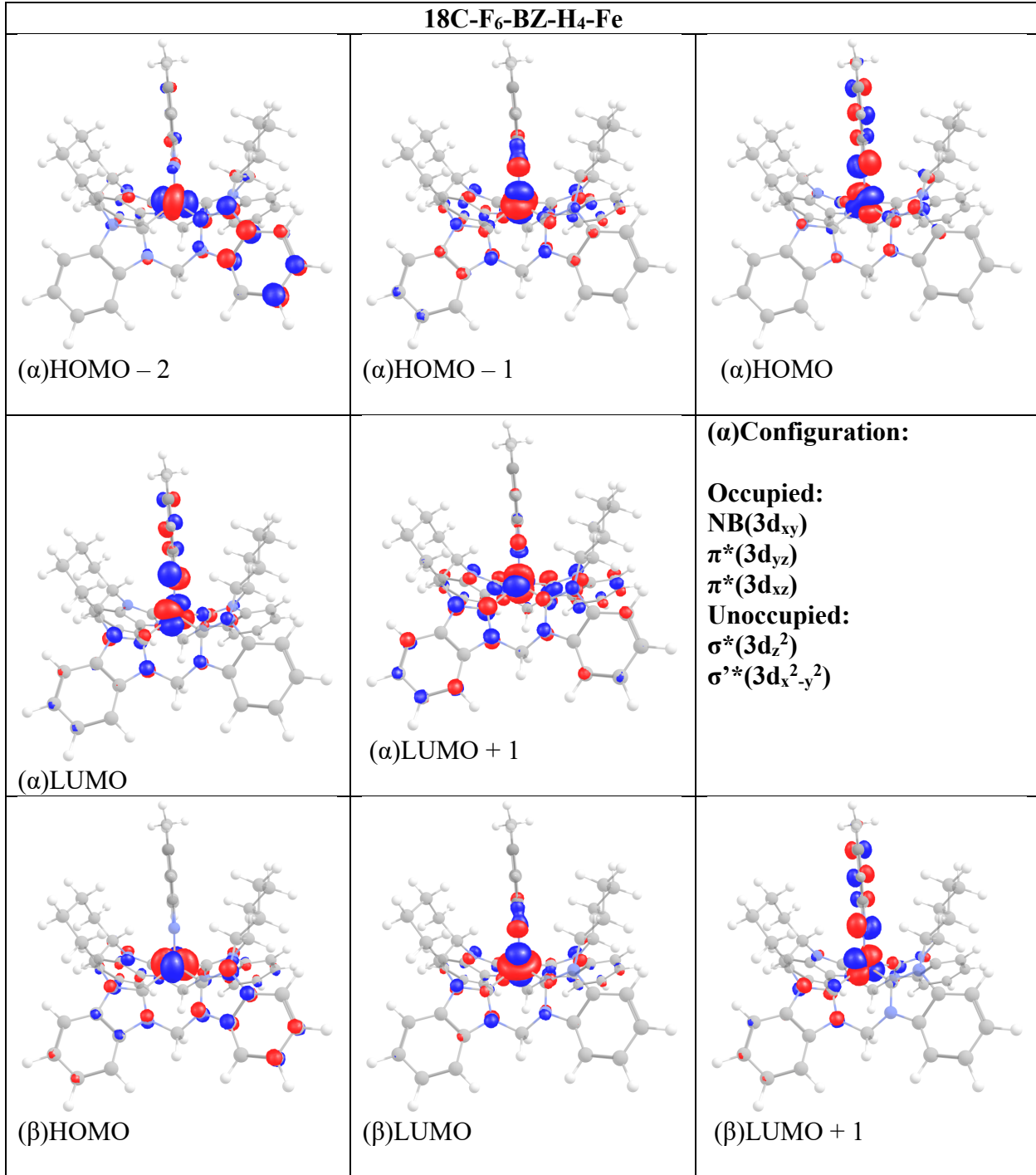
16C-W₂-BZ-H₄-Fe

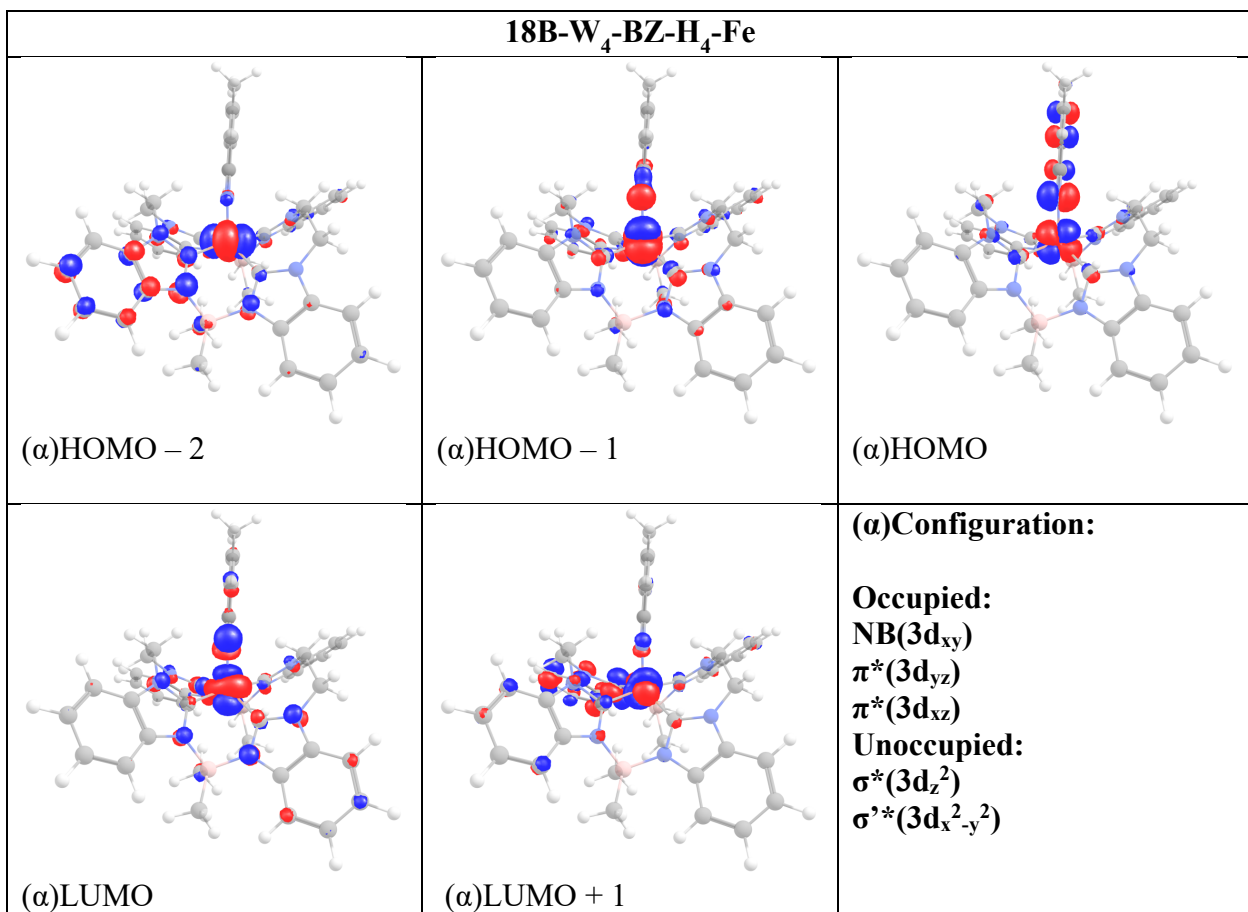
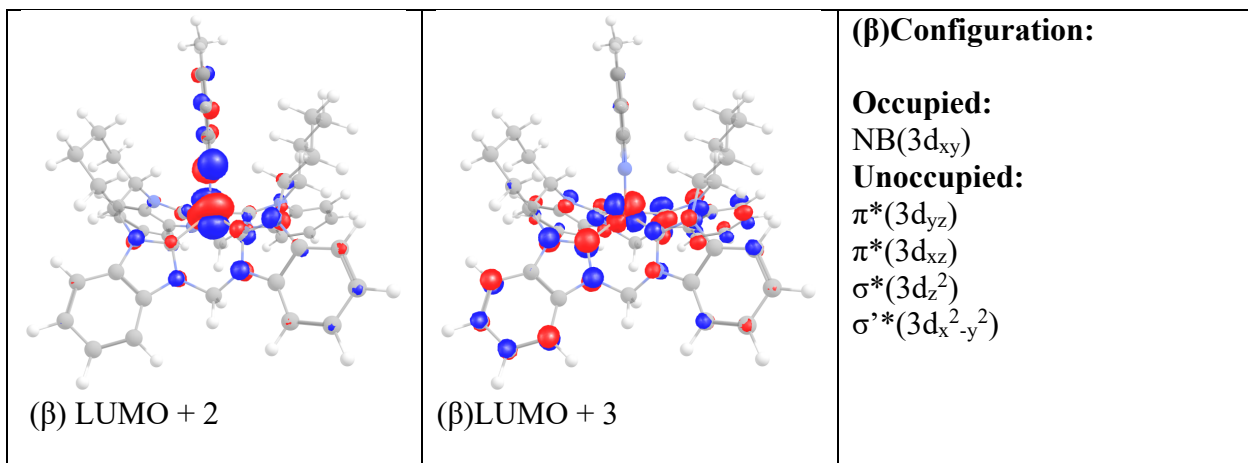


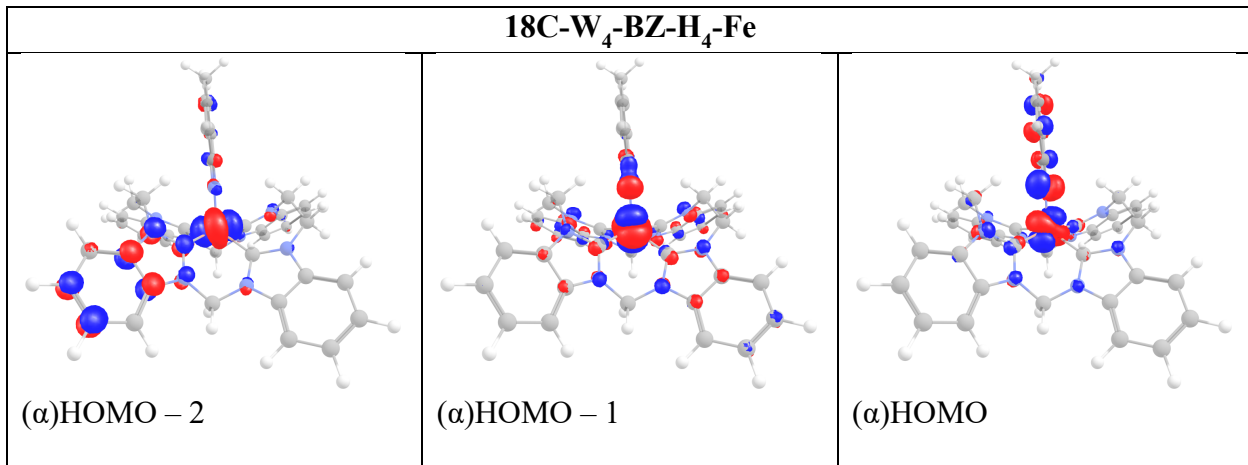
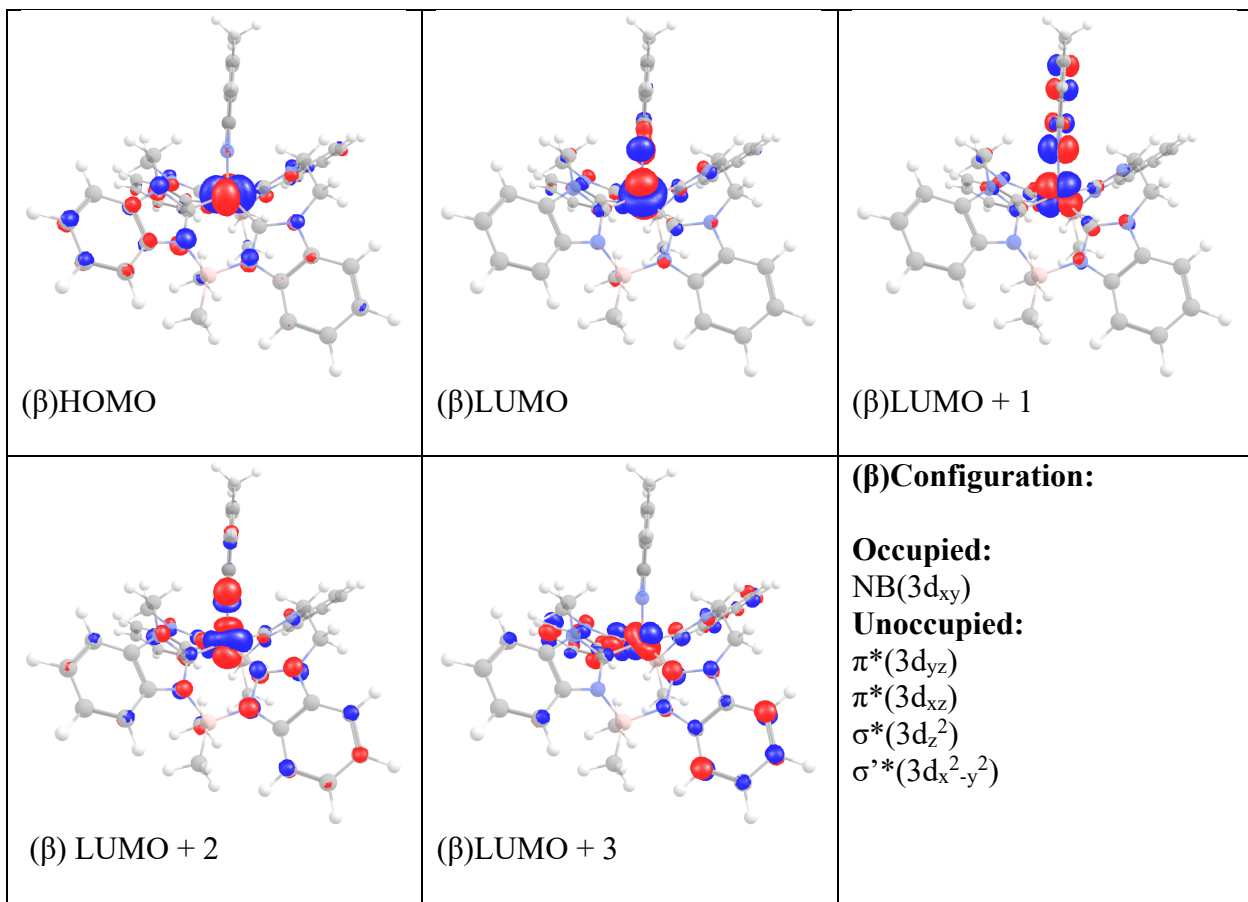


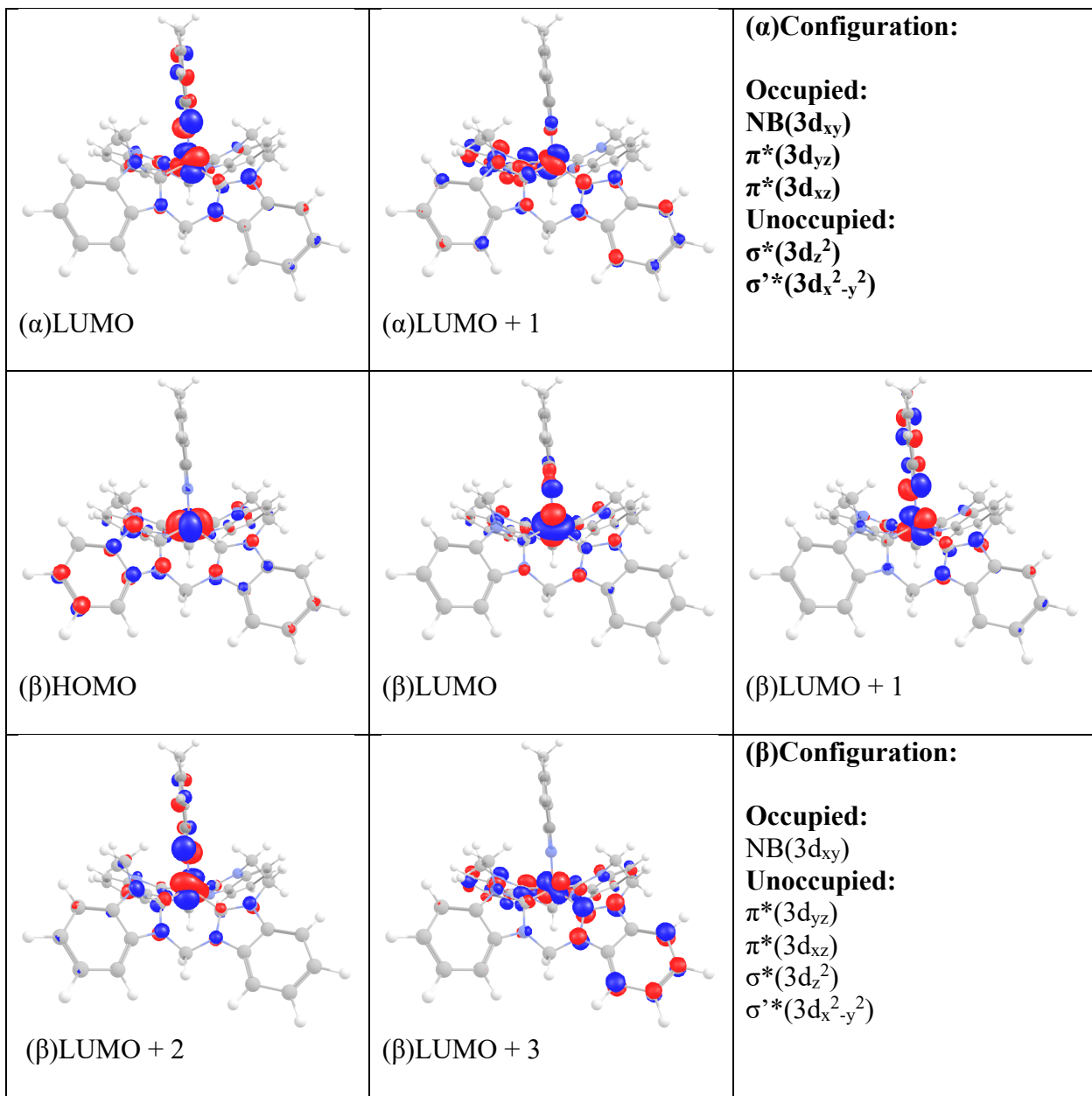


18C-F₆-BZ-H₄-Fe



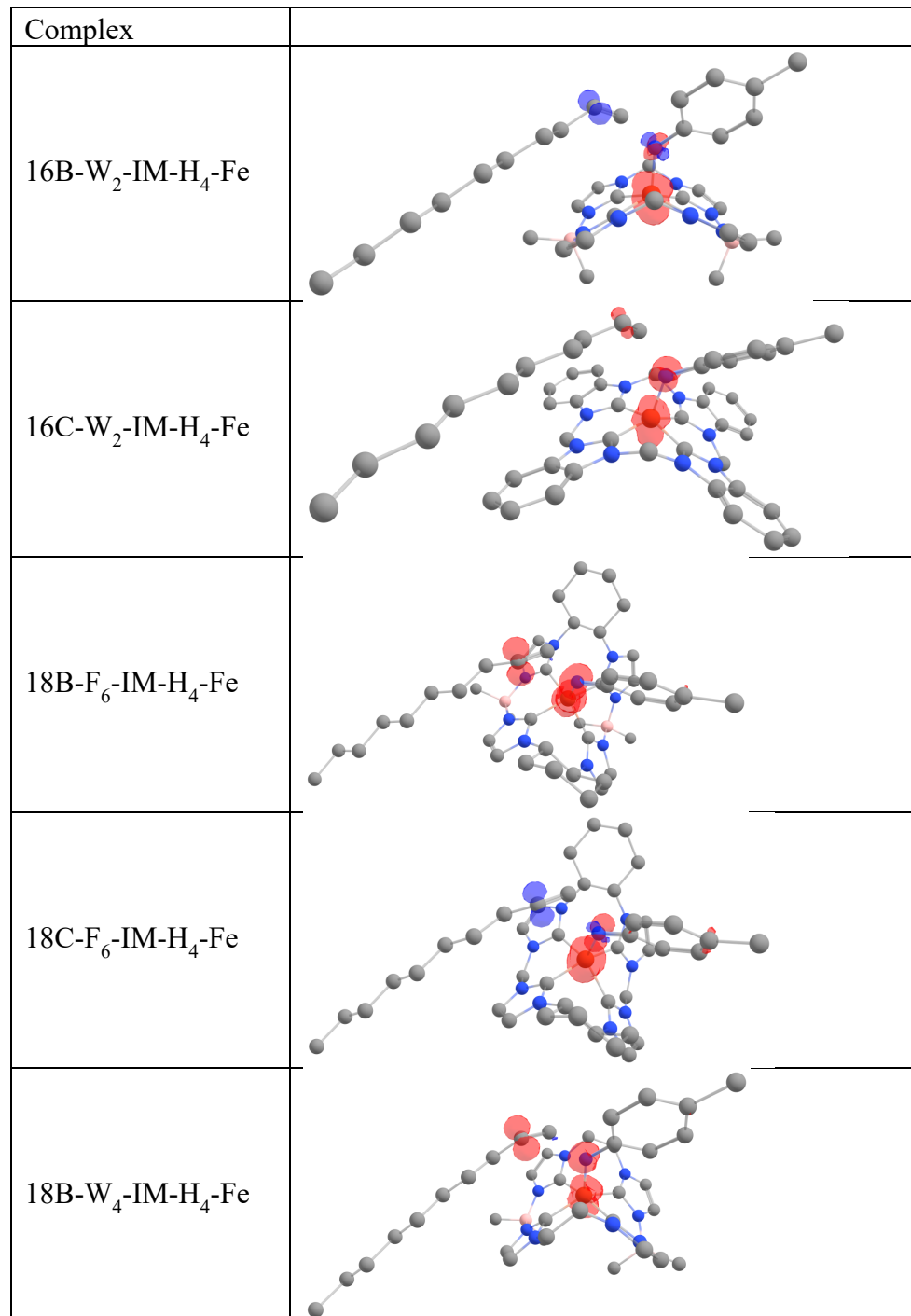


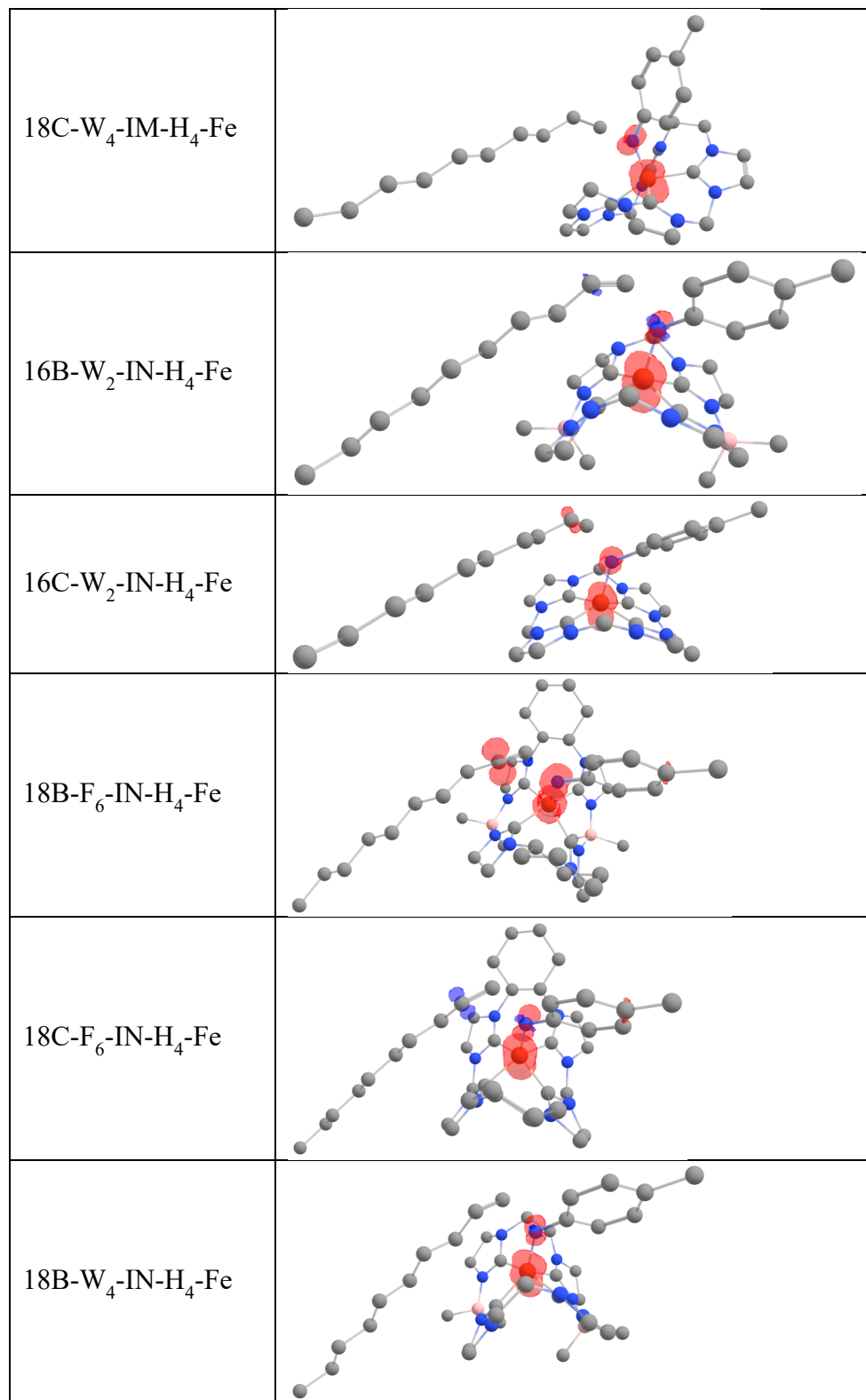


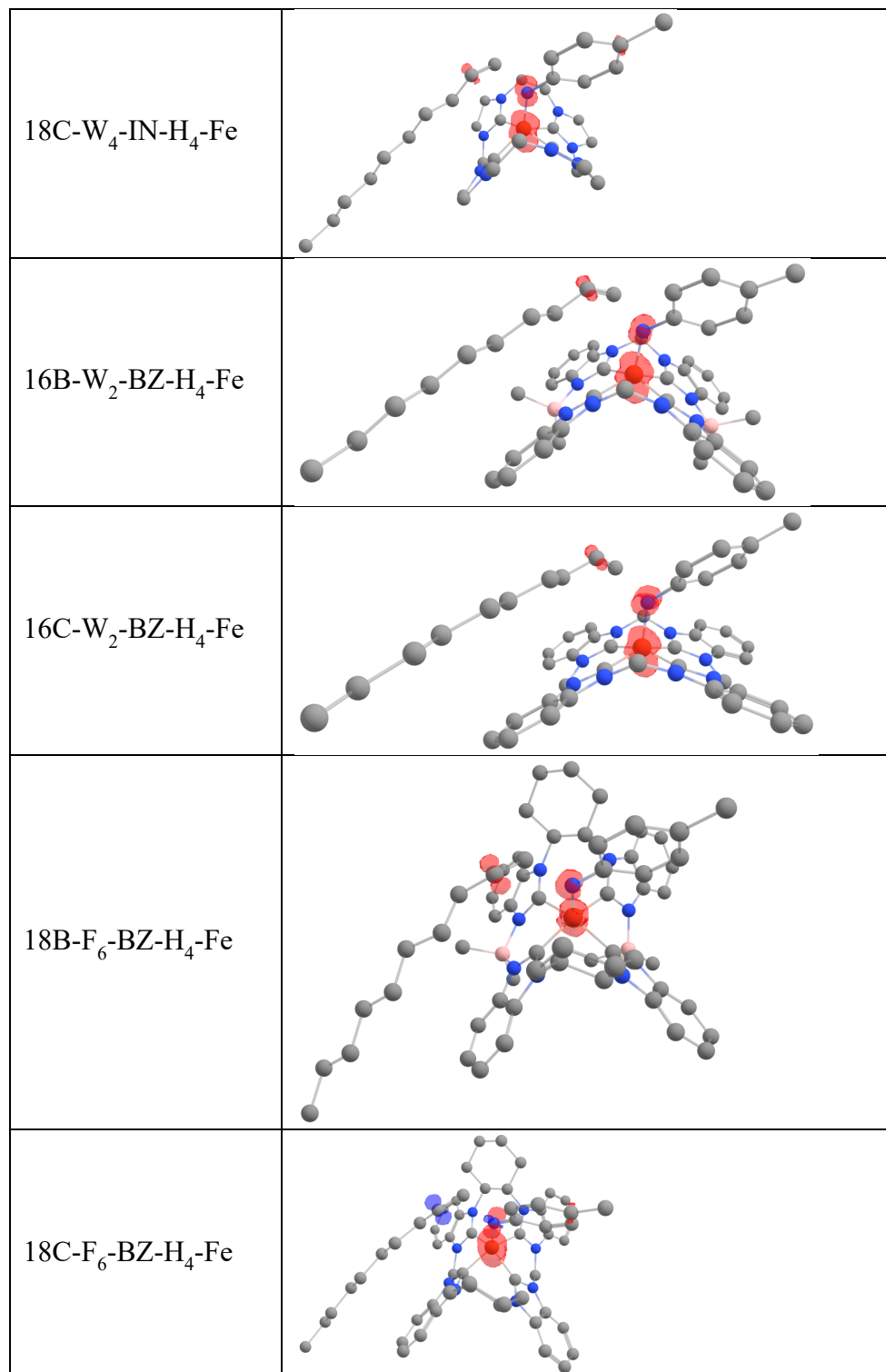


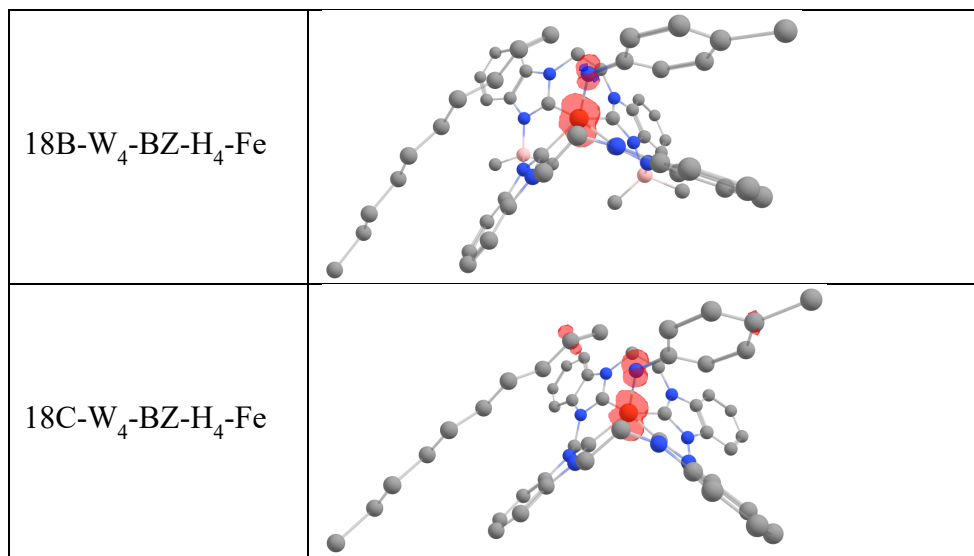
Section S3.2 Spin Densities

Spin densities displayed are from TS2 (alkene addition), all isosurfaces have been rendered at an isovalue of 0.08.









References

- (1) Neese, F.; Wennmohs, F.; Becker, U.; Ripplinger, C. The ORCA quantum chemistry program package. *The Journal of Chemical Physics* **2020**, *152* (22), 224108. DOI: 10.1063/5.0004608 (acccesed 9/25/2023).
- (2) Neese, F. Software update: The ORCA program system—Version 5.0. *WIREs Computational Molecular Science* **2022**, *12* (5), e1606. DOI: <https://doi.org/10.1002/wcms.1606> (acccesed 2023/11/28).
- (3) Perdew, J. P. Density-functional approximation for the correlation energy of the inhomogeneous electron gas. *Physical Review B* **1986**, *33* (12), 8822-8824. DOI: 10.1103/PhysRevB.33.8822.
- (4) Grimme, S.; Antony, J.; Ehrlich, S.; Krieg, H. A consistent and accurate ab initio parametrization of density functional dispersion correction (DFT-D) for the 94 elements H-Pu. *The Journal of Chemical Physics* **2010**, *132* (15), 154104. DOI: 10.1063/1.3382344 (acccesed 11/28/2023).
- (5) Grimme, S.; Ehrlich, S.; Goerigk, L. Effect of the damping function in dispersion corrected density functional theory. *Journal of Computational Chemistry* **2011**, *32* (7), 1456-1465. DOI: <https://doi.org/10.1002/jcc.21759> (acccesed 2023/11/28).
- (6) Eichkorn, K.; Treutler, O.; Öhm, H.; Häser, M.; Ahlrichs, R. Auxiliary basis sets to approximate Coulomb potentials (Chem. Phys. Letters 240 (1995) 283-290). *Chemical Physics Letters* **1995**, *242* (6), 652-660. DOI: [https://doi.org/10.1016/0009-2614\(95\)00838-U](https://doi.org/10.1016/0009-2614(95)00838-U).
- (7) Weigend, F.; Ahlrichs, R. Balanced basis sets of split valence, triple zeta valence and quadruple zeta valence quality for H to Rn: Design and assessment of accuracy. *Physical Chemistry Chemical Physics* **2005**, *7* (18), 3297-3305, 10.1039/B508541A. DOI: 10.1039/B508541A.

- (8) Hellweg, A.; Hättig, C.; Höfener, S.; Klopper, W. Optimized accurate auxiliary basis sets for RI-MP2 and RI-CC2 calculations for the atoms Rb to Rn. *Theoretical Chemistry Accounts* **2007**, *117* (4), 587-597. DOI: 10.1007/s00214-007-0250-5.
- (9) Blatchford, K. M.; Mize, C. J.; Roy, S.; Jenkins, D. M. Toward asymmetric aziridination with an iron complex supported by a D₂-symmetric tetra-NHC. *Dalton Transactions* **2022**, *51* (16), 6153-6156, 10.1039/D2DT00772J. DOI: 10.1039/D2DT00772J.
- (10) Isbill, S. B.; Chandrachud, P. P.; Kern, J. L.; Jenkins, D. M.; Roy, S. Elucidation of the Reaction Mechanism of C₂ + N₁ Aziridination from Tetracarbene Iron Catalysts. *ACS Catalysis* **2019**, *9* (7), 6223-6233. DOI: 10.1021/acscatal.9b01306.
- (11) Anneser, M. R.; Powers, X. B.; Peck, K. M.; Jensen, I. M.; Jenkins, D. M. One Macrocyclic Ligand, Four Oxidation States: A 16-Atom Ringed Dianionic Tetra-NHC Macrocycle and Its Cr(II) through Cr(V) Complexes. *Organometallics* **2019**, *38* (17), 3369-3376. DOI: 10.1021/acs.organomet.9b00476.
- (12) Anneser, M. R.; Elpitiya, G. R.; Townsend, J.; Johnson, E. J.; Powers, X. B.; DeJesus, J. F.; Vogiatzis, K. D.; Jenkins, D. M. Unprecedented Five-Coordinate Iron(IV) Imides Generate Divergent Spin States Based on the Imide R-Groups. *Angewandte Chemie International Edition* **2019**, *58* (24), 8115-8118. DOI: <https://doi.org/10.1002/anie.201903132> (accessed 2023/11/28).
- (13) Falivene, L.; Credendino, R.; Poater, A.; Petta, A.; Serra, L.; Oliva, R.; Scarano, V.; Cavallo, L. SambVca 2. A Web Tool for Analyzing Catalytic Pockets with Topographic Steric Maps. *Organometallics* **2016**, *35* (13), 2286-2293. DOI: 10.1021/acs.organomet.6b00371.
- (14) Lu, T.; Chen, F. Multiwfn: A multifunctional wavefunction analyzer. *Journal of Computational Chemistry* **2012**, *33* (5), 580-592. DOI: <https://doi.org/10.1002/jcc.22885> (accessed 2023/11/29).